ChemComm

FEATURE ARTICLE

View Article Online
View Journal | View Issue

Cite this: *Chem. Commun.*, 2025, **61**, 455

Atomically thin 2D materials for solution-processable emerging photovoltaics

Oleksandr Stroyuk, *[a] Oleksandra Raievska,[a] Jens Hauch[ab] and Christoph J. Brabec[ab]

Atomically thin 2D materials, such as graphene and graphene oxide, covalent organic frameworks, layered carbides, and metal dichalcogenides, reveal a unique variability of electronic and chemical properties, ensuring their prospects in various energy generation, conversion, and storage applications, including light harvesting in emerging photovoltaic (ePV) devices with organic and perovskite absorbers. Having an extremely high surface area, the 2D materials allow a broad variability of the bandgap and interband transition type, conductivity, charge carrier mobility, and work function through mild chemical modifications, external stimuli, or combination with other 2D species into van-der-Waals heterostructures. This review provides an account of the most prominent "selling points" of atomically thin 2D materials as components of ePV solar cells, including highly tunable charge extraction selectivity and work function, structure-directing and stabilizing effects on halide perovskite light absorbers, as well as broad adaptability of 2D materials to solution-based manufacturing of ePV solar cells using sustainable and upscalable printing technologies. A special focus is placed on the large potential of the materials discovery and design of ePV functionalities based on van-der-Waals stacking of atomically thin 2D building blocks, which can open a vast compositional domain of new materials navigable with machine-learning-based accelerated materials screening.

Received 30th September 2024,
Accepted 29th November 2024

DOI: 10.1039/d4cc05133e

rsc.li/chemcomm

1. Introduction

A cardinal shift in the modern paradigm of energy generation from traditional fossil fuels to renewable energy sources put forward the photovoltaic (PV) conversion of solar energy as one of the major players in future energy balance, along with other sustainable technologies, such as wind harvesting, hydrovoltaic and geothermal energy generation.[1–4] Recently, PV technologies crossed the terawatt (TW) generation threshold, with the current PV market dominated by silicon-based power-generating PV modules incorporating Si cells with *ca.* 24% power conversion efficiency (PCE).[1,3,5,6] The silicon-based PV technologies are universal and can be deployed at different scales, from vast multi-megawatt-peak (MWp) solar fields to small domestic farms, as well as in various applications – from building-integrated systems to semi-transparent agri-PV installations to automotive PV modules.[3,5,6] At the same time, the dominance of Si-based PV is associated with diverse economic and ecological risks, related both to the highly uneven distribution of manufacturing facilities and to a heavy burden of Si cell production and recycling on the environment.[3,6]

While currently PCE growth of Si-based PV modules has become incremental and is achieved mostly by optimizing manufacturing processes, future breakthroughs in PV harvesting of solar energy are expected from innovative emerging PV (ePV) technologies, capable of providing new alternative PV materials for scalable, ecologically benign, and localizable production of new-generation PV modules and realization of a broad scale of projects – from gigawatt (GW) to TW solar plants to specific products, such as integrated, semi-transparent, or flexible PV.[2,3,5,7–10] The field of ePV technologies encompasses both established alternatives for silicon, such as organic[5,8–11] and chalcogenide PV,[5,7,12] as well as "newcomer" materials, in particular, hybrid lead-halide perovskites.[3,7,10] The progress in ePV technologies is expected from several contributors, including the discovery of new light-harvesting and charge-collecting PV materials, optimization of the best of existing ePV materials and their upscaling to full-size modules, mitigation of environmental impacts by tailored recycling strategies, as well as from the development of innovative approaches to the manufacture of PV cells, allowing the environment-critical steps of Si-PV technology, such as Si purification, wafer growth, and segmentation, to be substituted by greener and sustainable alternatives. Among those, low-temperature printing of PV devices using solution-processed materials is considered one of the most promising venues.[13,14]

The realization of the complete cycle of low-temperature solar cell printing promises an immense boost for ePV because

[a] *Forschungszentrum Jülich GmbH, Helmholtz-Institut Erlangen Nürnberg für Erneuerbare Energien (HI ERN), 91058 Erlangen, Germany. E-mail: o.stroyuk@fz-juelich.de*
[b] *Friedrich-Alexander-Universität Erlangen-Nürnberg, Materials for Electronics and Energy Technology (i-MEET), Martensstrasse 7, 91058 Erlangen, Germany*

of compatibility with existing printing technologies and machinery, readily achievable up/down-scaling, and localization of the manufacture, as well as minimization of environmental pollution typically associated with mass production of Si cells.[3,6] On the other side, it brings new challenges, in particular, the need for specific materials – liquid inks, adaptable to various printing technologies and convertible into cell components, such as electron transport layers (ETLs), absorbers, hole transport layers (HTLs), back contacts, *etc.*, with no or minimal post-printing treatments. While the technologies of organic solar cells (OSCs) are already relatively well adapted to solution-based processes and can even be upscaled to roll-to-roll production,[8,9] the printing of perovskite solar cells (PSCs) would require the development of new solution-processable and environmentally stable ETL, HTL, and electrode materials that can be used to substitute thermal or vacuum deposition technologies and realize the complete cycle of PSC printing.[13,14]

Considering the large number of parameters to be optimized in ePV devices, including the cell stacking order and absorber type, the possibility of a precise tailoring of the electronic and chemical properties of printable charge-collecting layers becomes simultaneously a critical demand and a great challenge for solution-processed ePV. To meet this challenge, new types of charge-collecting materials should be considered, combining selective conductivity, optical transparency, chemical and electrochemical stability, broad and simple variability of basic properties, and solution-based processability, with all of these criteria potentially achievable in atomically thin 2D materials.

The emergence of 2D materials as a new direction of multidisciplinary research was heralded by the reports on the synthesis and properties of graphene by A. Geim and K. Novoselov, marked in 2010 by a Nobel prize in physics.[15,16] The rise of graphene had at least two important consequences, first, immediately revealing the large potential of graphene and its derivatives for various optoelectronic applications, including ePV, and, second, by inspiring a large-scale interest in atomically thin 2D materials in general, resulting in (re-)discovery of many new or under-appreciated 2D representatives of other classes, including inorganic chalcogenides, hydr(oxides), carbides, nitrides, organic covalent frameworks and others.[17–24] Atomically thin 2D materials (2DMs) showed large variability of many basic properties, for example, allowing for large variations in conductivity, charge carrier mobility, and work function (WF) by varying the number of layers and, for single layers, by covalent/non-covalent chemical modifications and dopings. Ultimately high surface-to-volume ratios typical for atomically thin 2DMs make their electronic characteristics easily affected by external stimuli, in particular, electrical fields and strains. The processability of solubilized 2DMs in liquid inks facilitates their incorporation into optoelectronic devices using sustainable low-temperature approaches.[17–24]

This tunability of properties ensured versatile applications of atomically thin 2DMs in light-harvesting technologies, including PV[17,19,22–63] and photocatalysis,[25,36,55,64–66] as well as in optoelectronics,[18,20,44,48,50,52,63,67–69] catalysis and electrocatalysis,[20,25,36,55,70–72] energy storage,[20,25,36,37,39,40,42,55,64,66,69–75] thermoelectrics,[36,74] sensors,[25,39,50,67,69,74,75] medicine,[40,64,70,71,73] *etc.* In the domain of potential ePV applications, high conductivity, charge carrier mobilities, optical transparency, processability and a broad variability of electronic properties of atomically thin 2DMs feature them as very promising materials for charge-selective ETLs/HTLs, absorber additives, electrodes, and interface layers.[22–24]

Though the potential of atomically thin 2DMs was recognized very fast, the practical implementation of their unique properties was limited by the labor-, time-, and energy-consuming character of many synthetic routes typically applied to produce and stack single-layer species, such as mechanical exfoliation or physical/chemical vapor deposition followed by substrate transfers.[56,63] In this view, solution-based processing of 2DMs appears as a very promising alternative as it combines mild, low-temperature, upscalable, and fast processing with the ease of integration with other components of ePV cells, tunability of rheological properties, and affinity to different substrates, as well as compatibility with the modern processing technologies such as spray coating and inkjet printing.[21,56,63]

In the analysis of the state-of-the-art applications of solution-processable atomically thin 2DMs in emerging PV, the present Feature article focuses on several selected classes of 2DMs, that dominate the ePV landscape and show considerable potential, including graphene and its derivatives such as graphene oxide and reduced graphene oxide, non-carbonaceous single-element 2DMs, in particular, antimonene and phosphorene, covalent organic frameworks, such as *p*olyheptazine carbon nitride, emerging metal-carbide MXenes, and transition metal dichalcogenides. These 2D compounds, though exemplifying vividly the benefits of versatile applications of atomically thin 2DMs in ePV, represent only a small selection from a much broader range of already available and theoretically possible 2D materials that hold promises for emerging PV technologies.

After focusing on selected 2DM materials, we discuss several aspects most critical for 2DM applications in sustainable solution-processed ePV, including (i) current applications of atomically thin 2DMs as components of PV absorbers, ETLs, HTLs, and interface additives in ePV systems, (ii) broad variability of the work function of atomically thin 2D ETL and HTL materials, (iii) potential of low-temperature solution-based production and processing of 2DMs in the form of liquid inks, and, finally, (iv) immense potential of materials discovery that can be provided by the combinatorial design of multi-layer and multi-component van-der-Waals heterostructures starting from a library of atomically thin ''building blocks''.

2. Introducing selected solution-processable 2D materials for ePV

This section provides a concise background for the selected 2D materials, outlining their properties crucial for ePV applications and their possible roles in ePV systems. The above-discussed selection of 2DMs to be surveyed as ePV materials is illustrated in Fig. 1a.

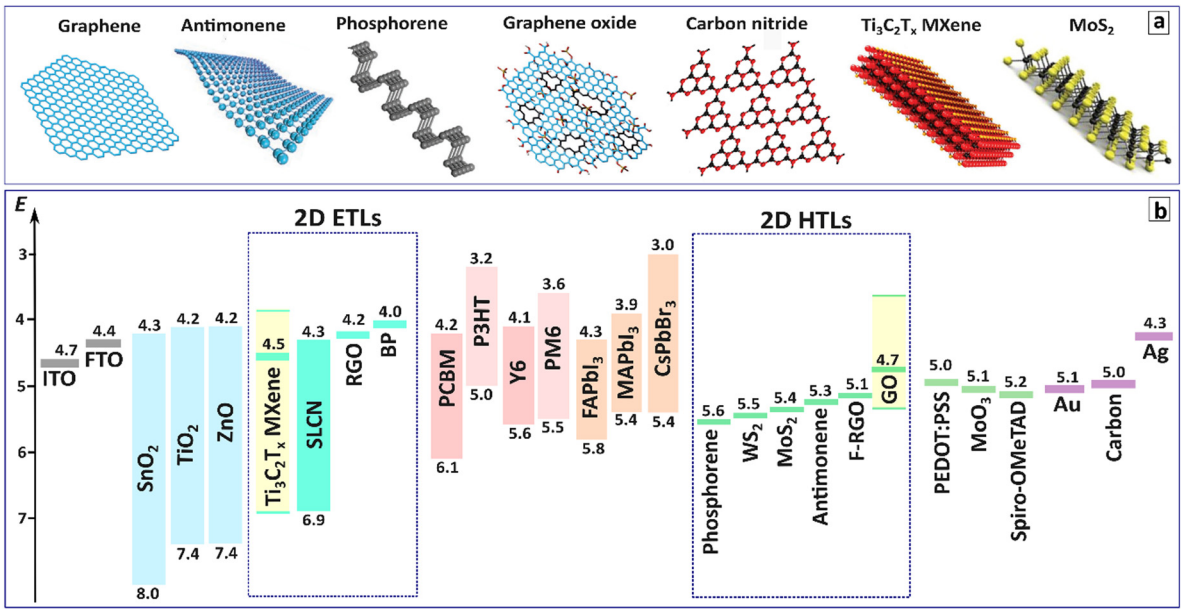

Fig. 1 (a) Stylized presentation of some of the PV-relevant atomically thin 2DMs. Reproduced with permissions from ref. 36, 40, 51, 65, 76 and 77. Copyrights: (2017) American Chemical Society; (2014, 2015, 2018, 2021, 2024) Wiley-VCH GmbH. (b) Energy levels of some typical TCEs, ETL and HTL materials, typical absorbers in OSCs and PSCs, as well as atomically thin materials used as ETL/HTL components. Sources of values: ITO,[78,79] FTO, TiO_2, Au, Spiro-OMeTAD,[80–82] ZnO,[83,84] SnO_2,[85] carbon,[86,87] Ag,[79,88,89] PEDOT:PSS,[78,83,90] MoO_3,[88] PM6,[83,85] Y6,[83] P3HT, PCBM,[91] MAPI,[79,82,92] FAPI,[86] $CsPbBr_3$,[87] $Ti_3C_2T_x$ MXene,[85,87] black phosphorus (BP),[81] single-layer PCN,[93] GO,[94,95] RGO,[95] antimonene,[92] phosphorene,[86] F-RGO,[96] MoS_2,[96,97] WS_2.[98] TCE, ITO, and FTO stand for a transparent conductive electrode, indium-tin oxide, and fluorine-doped tin oxide, respectively.

Graphene is a single layer of sp^2-bonded carbon atoms forming an infinite hexagonal 2D lattice and being an elementary unit of graphite, carbon nanotubes, and fullerenes.[22] Pristine (undoped, non-oxidized) graphene shows zero bandgap combined with high conductivity and charge carrier mobility (10^4–10^5 cm^2 V^{-1} s^{-1}), mechanical, chemical, and thermal stability, high flexibility, and tensile strength, high optical transparency (*ca.* 98%) and negligible reflectance.[20,22,51,99] Being only 0.33 nm thick and with all atoms formally on the surface, graphene is characterized by a theoretical specific surface area of more than 2600 m^2 g^{-1} and broad variability of work function (WF) through covalent and non-covalent modifications.[22,99] This combination of properties makes graphene an auspicious material for optoelectronic applications, particularly for ePV.[23,26–30,35]

Graphene oxide is an oxidized form of graphene typically produced by converting graphite into layered graphite oxide with strong oxidants ($KMnO_4$, $KClO_3$, *etc.*) followed by exfoliation into single-layer graphene oxide (GO) species.[20,22,23,26–35,44,57,61,62,76,99–101] GO sheets are decorated with various oxygen-containing functionalities (hydroxyl, carboxyl, carbonyl, epoxy, sulfonic groups) available for further covalent functionalization resulting in extensive processing opportunities and WF variations. Dielectric GO sheets can be converted into semiconductive/conductive form by thermal/chemical/photochemical reduction, eliminating functionalities and partially restoring graphene-like sp^2-hybridized honeycomb structure.[76,101]

Research of graphene stimulated broad interest in other single-element monolayer materials (also called Xenes, X = C, Si, P, Sb, *etc.*), in particular, antimonene[25,61,70,71,73,102] and phosphorene,[20,22,23,36,37,56,57,59–61,64,74,103–106] both showing promises for emerging PV applications.

Antimonene is a 0.6-nm thick single layer of antimony showing semiconductor behavior with an indirect bandgap of *ca.* 2.3 eV. Antimonene reveals a strong dependence of electronic properties on the number of layers, with a bandgap closing to zero already for bi-layer and showing metallic character for thicker stacks.[25,61,71,73,92,102] Similar behavior was predicted for bismuthene,[61,107] however, experimental research on single-layer Bi is still to be reported.

Single-layer phosphorene can be produced by exfoliation of layered phosphorus allotrope – black phosphorus (BP).[20,36,56,64,103,105] Similar to other Xenes, single-layer phosphorene is a semiconductor with a bandgap of 2.0 eV, that decreases with an increase in the layer number down to 0.3 eV for bulk BP.[20,64] Single-layer phosphorene has a thickness of 0.53 nm and a honeycomb structure with non-planar structural ridges resulting in strong anisotropy of electronic and optical properties.[20,36,56] Phosphorene is characterized by high hole mobility on the order of 10^3 cm^2 V^{-1} s^{-1} (ref. 20, 64 and 103–105) and intrinsic ambipolar behavior[103] making it a promising material for both ETL and HTL applications in ePV.

Different types of covalent organic frameworks form graphene-like infinite 2D networks capable of staking into layered graphite-like materials, in particular polyheptazine carbon nitride (PCN), polytriazine carbon nitride, or polytriazine imide (PTI), many of them known since Liebig's experiments with melon in 19th century.[100] These layered solids show stronger interlayer forces than graphite but can still be exfoliated into corresponding single and a-few-layer atomically thin sheets.

Polyheptazine carbon nitride is one of the most stable modifications forming infinite 2D networks of heptazine heterocycles stacking into graphitic PCN that shows semiconductor behavior with a bandgap of *ca.* 2.7 eV and positions of conduction (CB) and valence bands (VB) favorable for PCN to serve as an excellent photocatalyst in the processes of artificial photosynthesis, such as water splitting, and CO_2 and N_2 reduction.[54,55,63,65,66,108] The structure of PCN sheets can be broadly tuned by doping, atomic substitutions, chemical functionalization, and morphology engineering both during the formation of bulk graphitic PCN and after the exfoliation to atomically thin PCN sheets.[54,55,66] Single-layer PCN has a thickness of *ca.* 0.34 nm, a theoretical specific surface area of *ca.* 2500 $m^2\ g^{-1}$, and low electrical conductivity of *ca.* 1 S cm^{-1}.[55,65]

After first reports on the synthesis of atomically thin 2D transition metal carbides, nitrides, and carbonitrides, generally called MXenes with a brutto-formula of $M_{n+1}X_nT_x$ (n = 1–3, M – metal, X = C, N, C + N, T – functionalities such as F or OH) in 2011, the chemistry of MXenes experienced rocketing development with a current opinion about the MXenes as one of the most promising classes of 2D materials.[22,38–47,57,60–62,75,106,109,110] Among the most broadly studied MXenes are $Ti_3C_2T_x$ and Nb_2CT_x with metallic conductivity and $Mo_2TiC_2T_x$ semiconductors.[40,46,75] Atomically thin MXenes can be produced by etching of the so-called MAX phases, $M_{n+1}AX_n$, with the most frequent A = Al. Presently, over 100 MAX phases were synthesized and etched to yield 46 MXene compounds, many of them showing outstanding conductivity, tunable surface functionality, variable work function, high optical transmittance, hydrophilicity, and solution processability.[40,41,45,111] Conversion of MAX phases into MXenes is typically achieved by etching Al^{3+} with HF or alternative fluorine-containing agents. Practical applications of MXenes have recently received an additional impetus due to the development of sustainable and scalable fluorine-free syntheses.[45,111,112]

Along with MXenes, fast progress is observed in the chemistry and applications of atomically thin and single-layer transition metal dichalcogenides (TMDCs) with $MoS(Se)_2$ and $WS(Se)_2$ as the most broadly studied representatives.[22,48–53,57–62,67,69,99,106] Single TMDC layers are formed by covalently bound metal and chalcogens, while separate layers are stacked due to van-der-Waals forces.

Single-layer MoS_2 with a thickness of *ca.* 0.7 nm showed a plethora of unique properties, including an outstanding mechanical strength and Young's modulus higher than that of steel, as well as high charge carrier mobility of up to 200 $cm^2\ V^{-1}\ s^{-1}$, making it highly promising for applications in flexible optoelectronic devices.[48–52] TMDCs, in particular, MoS_2 and WS_2, show spectacular bandgap dependences on the layer number, revealing indirect bandgaps as bulk solids and direct bandgaps as single layers.[49,52,67,113,114] At that, the bandgap of MoS_2 was reported to increase from 1.2 eV for bulk solid to 1.8–1.9 eV for a single MoS_2 layer.[49,52,67] Simultaneous shifts of the CB/VB positions as well as exciton binding energy result in a strong dependence of photophysical and ground-state redox properties of atomically thin MoS_2 on the layer number.[99,115]

As discussed in Section 3, these selected 2DMs have the highest potential as charge collection layers (ETLs or HTLs) of ePV devices with organic or hybrid perovskite absorbers. The charge carrier selectivity depends on the type of conductivity and Fermi level of 2DMs and in many cases can be varied so broadly by chemical treatments and dopings as to allow the same 2DM to be applied both as ETL or as HTL material, depending on the 2DM processing history.

Fig. 1b provides a comparative "map" of electron levels of some conventional absorbers, ETL, and HTL components of organic and perovskite solar cells along with the typical positions of acceptor/donor levels of selected atomically thin 2DMs. This map is only intended to provide an illustration of exemplary cases of 2DMs applied as ETLs and HTLs, rather than to assign static roles to specific 2D materials. As we discuss in Section 4, the variability of the work function of most of the 2DMs presented in Fig. 1b is very broad, allowing the WF level to be tuned "on demand" and even switch between ETL and HTL roles for the same 2D materials by tailoring their surface chemistry and electron density distribution. This WF variability is exemplified in Fig. 1b for the cases of $Ti_3C_2T_x$ MXene ETL and GO HTL, where the scope of reported WF values is shown by yellow bars to provide an idea of the variability range. We refer the readers for more details on the WF design to Section 4.

3. Multiple roles of 2DMs in ePV applications

Atomically thin 2D materials find applications in all components of ePV devices, including absorber layers, charge-selective transport layers (ETL and HTL), and various interface layers. Along with those roles, highly conductive and transparent graphene was also reported as a good candidate for transparent electrodes, especially on flexible substrates.[22,23,26–30,33,34,61–63,98,99] In the following discussion, we focus consecutively on multiple roles of 2D materials introduced into the light-harvesting layer as well as into ETL and HTL components.

3.1. 2D materials in ePV absorbers

Considering their ultimately low thickness, single- and a-few-layer 2DMs reveal intense light absorption. In particular, graphene absorbs 2.3% of visible light being only *ca.* 0.3 nm thick,[17,18,26,28–30,62,99] while for silicon comparable absorbance can be achieved for a 20-nm thick Si layer.[116] Single-layer TMDCs, such as MoS_2 and WS_2, can absorb 5–10% of incident solar light and, when combined into excitonic cells or with graphene into Schottky-junction cells, they potentially can show 1–3 orders of magnitudes higher power density as compared to the best thin-film solar cells.[17,18,51,53,99,116] Still, this level of absorbance can be exploited only in exotic devices, for example, in nearly transparent solar cells based on WS_2 monolayers,[117] while thicker multilayer TMDC films typically reveal high reflectivity requiring additional light-trapping approaches to be introduced.[17]

In practice, atomically thin 2D materials are mostly introduced as additives to more conventional absorbers, such as organic bulk heterojunctions (BHJs) or lead-halide perovskites to modify their properties. In the case of OSCs, 2D materials, such as the antimonene bilayer[118] can be introduced to enhance exciton dissociation and reduce charge recombination between the BHJ components. In PSCs, 2D additives play multiple roles, altering the morphology of the perovskite absorber layer, passivating grain boundaries, aligning energy levels of charge-selective layers and perovskite absorber, suppressing ion migration, redox-reactions on interfaces, and moisture penetration.

3.1.1. PSCs – active layer morphology. By their influence on perovskite morphology, atomically thin 2DMs resemble self-assembled molecular monolayers,[119] that tune the hydrophilicity of the surface and density of nucleation centers.[19,22,60] In particular, antimonene films deposited on SnO_2 ETL provide nucleation sites for the growth of formamidinium lead iodide (FAPI) crystals resulting in vertically oriented growth of larger absorber grains extending from ETL up to HTL with no grain boundaries parallel to the substrate (Fig. 2a).[120] 2D materials pre-deposited on ETL/HTL components induce more homogeneous nucleation and growth of lead-perovskite crystals, generally resulting in larger grains and the formation of much uniformer and denser absorber films (Fig. 2b and c). The positive effects on perovskite grain size and film uniformity were reported for GO (Fig. 2b),[90] antimonene,[92,120] bismuthene,[97] MXenes (Fig. 2c),[41–43,45,47,121–124] and ultrathin PCN layers.[54,125,126]

The introduction of MXenes in the PbI_2 layer during the two-step perovskite deposition produces a system of pores facilitating subsequent diffusion of MAI and formation of a uniform perovskite layer with no PbI_2 residuals.[121]

3.1.2. PSCs – grain passivation and interfaces. Interaction between lone electron pairs of the basal plane and/or functional groups of 2D sheets with perovskites results in passivation of undercoordinated Pb(II),[19,60] suppressing defect-related recombination, and contributing considerably to overall PCE enhancement observed for antimonene,[120] phosphorene,[82] MXenes,[45,47,121,127,128] PCN,[54,125,129] and PTI additives.[130] 2DM sheets form heterojunctions with perovskite grains facilitating exciton dissociation and charge extraction, as reported for WS_2[131] and MXenes.[128] A pump-and-probe study of MAPI/WS_2 (MAPI is methylammonium lead iodide) indicated that charge separation between components is extremely fast and occurs within 50 fs.[131] When placed between ETL and perovskite absorber, 2D additives, in particular, antimonene,[120] bismuthene,[97] MXenes,[47,128,132] and PTI,[130] modify energy level alignment on the perovskite/ETL interface, increasing the efficiency of electron extraction and electron mobility, as well as blocking the hole extraction by ETL.

3.1.3. PSCs – stability. Interaction with functional groups of 2D additives, in particular, PTI,[130] suppresses ion migration in PSCs resulting in enhanced stability. Generally, PSCs with 2D additives reveal much higher environmental stability and shelf-storage time as compared to corresponding unmodified cells due to a combination of grain passivation, suppressed ion migration, and mitigated moisture ingress. Stability enhancement was reported for antimonene (Fig. 2d),[120] bismuthene,[97] and MXene[45,47,128] additives. Atomically thin C_3N_3 and C_3N_5 sheets were reported to suppress redox reactions between NiO_x HTL and

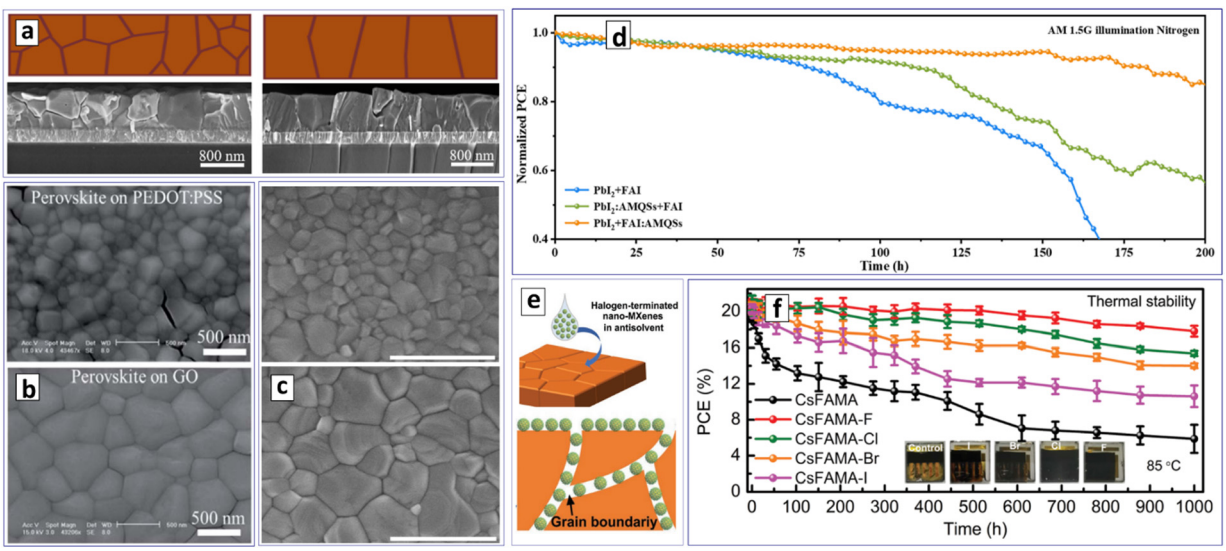

Fig. 2 (a)–(c) Influence of 2D additives on the morphology of perovskite absorbers. The figure shows a schematic grain structure of the perovskite layers in the upper panel (left – without additives, right – with antimonene sheets) with cross-sectional SEM images of corresponding layers on ITO substrates on the lower panel. (b) and (c) SEM images of perovskite layers formed on ITO substrates (upper images) and pre-deposited layers of 2D materials (lower images); 2DM is GO in (b) and MXene in (c). (d) and (f) Examples of the influence of 2D additives on the stability of perovskite-based solar cells. (e) Scheme showing perovskite grain passivation by MXene nanoparticles. In (f) FA, MA – formamidinium and methylammonium cations. Reproduced with permissions from ref. 120 (a) and (d), ref. 90 (b), ref. 121 (c), and ref. 127 (e) and (f). Copyrights: (2023) American Chemical Society (a) and (d); (2017) The Royal Society of Chemistry (b); (2020) Elsevier B.V. (c); (2022) Wiley-VCH GmbH (e) and (f).

perovskite absorber.[133] Nanoparticles of halogenated MXenes confined in grain boundaries of the FAPI absorber (Fig. 2e) form Pb–halogen bonds with perovskite grains increasing the stability of the cells dramatically even in harsh conditions of the damp/heat tests.[127] Such cells maintain 85% of PCE after 1000 h operation under thermal stress at 85 °C with no additional encapsulation (Fig. 2f).[127]

3.2. Atomically thin 2D materials as ETL components in ePV

Many conductive and semiconductive atomically thin 2D materials with WF below 5 eV were reported to perform excellently as ETL materials or additives to conventional ETLs in organic and perovskite solar cells, the most popular 2DM ETLs including graphene,[22,26–30,33,57,62,99,134] reduced GO,[27,28,30–34,62,99] phosphorene,[36,37,57,60,106] MXenes,[38–43,45–47,57,60,62,75] and PCN[54] (Fig. 1b).

The introduction of graphene into the network of mesoporous titania ETL in PSCs was reported to increase the electron collection capacity by a factor of 3.[134] In a similar system, lithium-neutralized graphene oxide deposited over mesoporous titania ETL enhanced the electron transfer from perovskite absorber and increased the device photostability by passivating oxygen vacancies of TiO_2 ETL.[80] Combining titania with phosphorene sheets allows the PSCs to be produced using low-temperature processing conditions reaching PCEs comparable with those observed for conventional ETL annealing.[81]

The addition of highly conductive Ti- and Nb-based MXenes to metal oxide ETLs in ePV cells typically enhances the conductivity and electron collection capacity of the transport layers,[40,45–47,84,122,135] at the same time mitigating the photocatalytic activity of oxide ETL materials.[84] In the case of PSCs, composite TiO_2/MXene ETLs showed enhanced performances both for lead-halide and lead-free halide perovskite absorbers, such as $Cs_2AgBiBr_6$.[135]

Suppression of the photocatalytic activity of oxide ETLs by MXenes was found to be especially tangible for BHJ OSCs, where photodegradation at the BHJ/ZnO interface under UV illumination is one of the major instability issues. At that, ZnO/MXene-based OSCs show PCEs comparable to those of ZnO-only counterparts but demonstrate enhanced general photostability (Fig. 3a).[84]

Deposition of $Ti_3C_2T_x$ MXene on SnO_2 ETL passivates grain boundaries of the oxide layer and creates a much smoother surface, positively affecting the quality of perovskite absorber layers, in particular, eliminating pinholes and reducing the trap density.[85] First-principles calculations indicated electron hybridization between SnO_2 and MXene layers resulting in enhanced electron mobility and electron extraction efficiency of composite SnO_2/MXene ETL, manifesting in a strong reduction of the radiative lifetime in the perovskite absorber (Fig. 3b).[85]

Recently, the feasibility of using individual $Ti_3C_2T_x$ MXenes as ETL was reported, opening a new route to low-temperature solution-processing of planar PSCs using liquid MXene inks.[79] Before MAPI absorber deposition, MXene layers on ITO were subjected to UV/ozone treatment, resulting in partial conversion of Ti–C bonds into Ti–O bonds. This treatment strongly enhanced the bonding between ETL and perovskite, at the same time not affecting the vital properties of MXene, such as conductivity and high electron mobility, resulting in a large increase in PCE.[79]

The introduction of a partially oxidized $Ti_3C_2T_x$ MXene layer between Ag/fullerene-based ETL and $CsPbI_3$ perovskite generates an additional electric field on the absorber/ETL interface strongly enhancing electron collection and simultaneously providing a physical barrier for moisture ingression.[136] Such stack was used to produce small cells with PCE of almost 20% as well as 25 cm^2 minimodules showing efficiencies close to 15% and remarkable stability during a 1000-h damp/heat test under AM1.5G illumination (Fig. 3c).[136] In a similar system based on partially oxidized Nb_2CT_x MXene, an almost 3% PCE increment was achieved for composite SnO_2/MXene ETL, the devices showing less than 15% PCE loss after 1500-h of shelf storage.[124]

Atomically thin polyheptazine carbon nitrides can be applied as efficient ETL materials both for OSCs and PSCs providing unique opportunities for tailoring WF and interactions with other cell components by chemical functionalization.[54,93,126] In OSCs, self-assembled PCN layers formed by stacked single-layer PCN sheets were reported to be as efficient ETL as conventional nanocrystalline ZnO, at the same time showing a higher transparency and a lower light scattering, resulting in higher external quantum efficiency (EQE) over most of the tested spectral range (Fig. 3d).[93] The introduction of sulfur-doped PCN between SnO_2 ETL and perovskite absorbers results in considerably reduced recombination on the ETL/perovskite interface due to passivation of the undercoordinated Pb^{2+} by sulfur atoms of PCN interlayer.[126]

3.3. Atomically thin 2D materials as HTL components in ePV

Interest in semiconducting 2D materials with relatively high WF (*ca.* 5 eV and higher, Fig. 1b) as HTL components of ePV cells is stimulated by their chemical and photochemical stability and promising hole-transporting and electron-blocking characteristics. These characteristics make 2DMs a viable alternative to conventional HTLs such as PEDOT:PSS (poly(3,4-ethylenedioxythiophene):polystyrene sulfonate) or Spiro-OMeTAD (N^2,N^2,$N^{2\prime}$,$N^{2\prime}$,N^7,N^7,$N^{7\prime}$,$N^{7\prime}$-octakis(4-methoxyphenyl)-9,9′-spirobi[9H-fluoren]-2,2′,7,7′-tetramin), notoriously known for their limited hole conductivity and low stability. Similar to the above-discussed case of ETLs, 2D HTLs, such as oxidized graphite,[26–30,33,137] GO and derivatives,[22,26–30,32,34,57,62,78,90,91,94,95,107,138,139] antimonene,[25,92,140] phosphorene,[23,36,37,57,59,60,86,106,137] PCN,[54,141,142] MXenes,[40–43,45–47,57,60,62,75,87,106,123,143,144] and TMDCs,[22,23,49–51,53,57–60,62,89,96,99,106,145,146] provide multiple possibilities of variations of chemical and electronic properties and can be introduced into ePV cells using solution-processing approaches.

Single-layer graphene oxide was reported as an alternative for PEDOT:PSS HTLs in P3HT/PCBM-based OSCs (P3HT is poly(3-hexylthiophene-2,5-diyl), PCBM is phenyl-C_{61}-butyric acid methyl ester) as early as 2010, the GO-based devices showing the same efficiency, but much higher stability.[138] The hole-extraction efficiency of GO can be controlled by partial

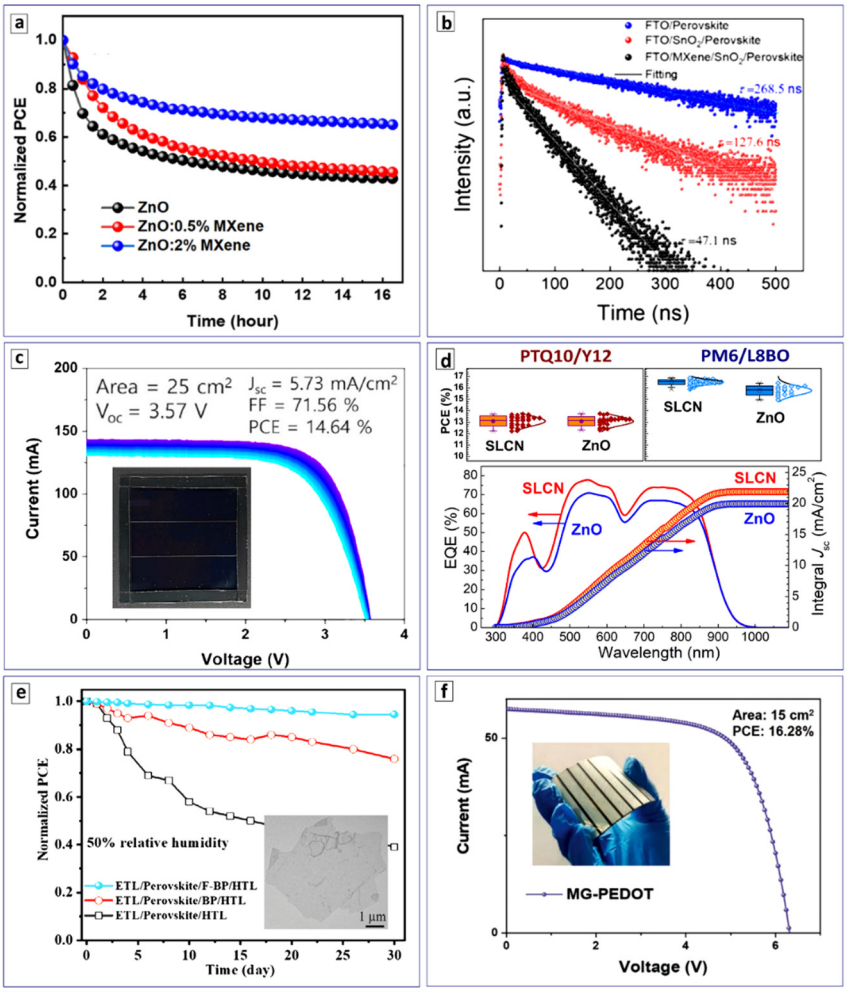

Fig. 3 (a) Evolution of PCE of OSCs with ZnO and ZnO/MXene ETLs; (b) PL decay traces for perovskite combinations with different ETL materials; (c) evolution of *I*–*V* curve of encapsulated PSC minimodule under damp-heat and 1-sun illumination registered for 1000 h; insert shows a photograph of the minimodule; (d) upper panel – PCEs of OSCs with two different BHJs and single-layer carbon nitride (SLCN) and ZnO as ETLs; lower panel – EQE spectra and integral J_{sc} calculated from EQE spectra for a PTQ10/Y12-based cell with SLCN and ZnO ETLs; (e) evolution of PCE of PSCs with different HTLs during shelf storage; insert shows a TEM image of a phosphorene sheet; (f) *I*–*V* curve for a flexible PSC minimodule with a MoS_2/PEDOT:PSS HTL; insert shows a photograph of the minimodule. Reproduced with permissions from ref. 84 (a), ref. 85 (b), ref. 136 (c), ref. 137 (e), and ref. 123 (f). Copyrights: (2020, 2023) American Chemical Society (a) and (b); (2022) Elsevier Inc. (c); (2022) Wiley-VCH GmbH (e) and (f).

reduction[91,95,139] as well as variations in the HTL thickness to balance WF and conductivity.[90,94,95,138] Additionally, GO provides a versatile functionalization chemistry, allowing the processability and electrical properties of the 2DM to be finely tuned. In particular, the decoration of GO sheets with $-OSO_3H$ groups results in higher solubility for ink preparation and almost three orders of magnitude increase in conductivity.[94] Fluorinated GO was used individually and combined with PEDOT:PSS HTL, the mixture resulting in a higher PCE than individual PEDOT:PSS.[78] The latter example is of special interest for low-temperature processing of OSCs as it reports stable F-GO inks and a Field-metal back electrode formed in an open environment without thermal vacuum deposition.[78]

Antimonene sheets were tested as additives to HTL components of OSCs[25,102,140] and PSCs[25,92] showing multiple benefits, such as increased hole conductivity, better contact to absorber layers, and suppression of side reactions between the absorber and HTL.[92,140,147]

Atomically thin phosphorene is characterized by a high hole conductivity and environmental stability making it a promising HTL material for PSCs.[86,137] Perovskite cells with phosphorene HTLs showed PCE over 15% and V_{oc} higher than 1 V attesting to a high potential of this charge transport material.[86] Fluorinated phosphorene can passivate undercoordinated Pb^{2+} and provide a smoother energy level alignment between the absorber and a Spiro-OMeTAD HTL. At the same time, it shows excellent humidity resistance, contributing to a dramatic enhancement of the PSC stability (Fig. 3e).[137]

The introduction of $Ti_3C_2T_x$ MXene flakes into PEDOT-PSS HTLs increases the hole extraction efficiency, hole conductivity, and mechanical stability of HTL, making it a promising choice for flexible PSCs.[123] An example of a flexible 15-cm^2 perovskite

solar module with a PCE of *ca.* 16% was demonstrated with HTL printed by blade-coating from a liquid MXene-PEDOS:PSS ink (Fig. 3f).[123] A mixed Nb_2CT_x MXene/PEDOS-PSS HTL was developed for ternary OSCs showing maximal PCE of *ca.* 19%.[144] MXenes showed a high potential as interlayers between perovskite absorber and carbon back electrodes in all-inorganic PSCs.[87,148]

Transition metal dichalcogenides, in particular, MoS_2 and WS_2, were recognized as promising substitutes for conventional HTLs in OSCs[49–51,53,89,96,146] and PSCs,[49–51,53,145] that can be readily adapted for solution-processed ePV using liquid-phase exfoliation approaches discussed in Section 5. Even an ultra-thin single-layer MoS_2 (0.67 nm thick) can be an efficient HTL for PSCs, showing PCE higher than 20% for an inverted device with ITO/MoS_2/MAPI/TiO_2/Ag configuration.[145] Thicker flakes of MoS_2 (2–8 single layers) and WS_2 (2–4 single layers) stabilized in liquid inks, as well as graphene/MoS_2 bilayer composites[89] were probed as HTLs in OSCs matching PEDOT:PSS in hole extraction efficiency.[96,146]

The addition of polyheptazine carbon nitride sheets strongly enhances the conductivity of PEDOT:PSS, allowing non-fullerene OSCs to be manufactured with a reduced HTL thickness and higher transmittance, resulting in tangible PCE increments.[141] The introduction of PCN as an interlayer between NiO_x HTL and perovskite absorber enhances cell stability due to the suppression of redox reactions between nickel oxide and iodide anions.[142]

4. Work function design in 2DMs

Atomically thin 2D materials show broad variations of electronic properties, in particular, work function and charge carrier mobility, enabling their applications both as electron- and hole-transporting layers as discussed in Sections 2 and 3. This variability stems from a high sensitivity of electron density distribution in 2DMs on their chemical composition, doping, and number of layers, on effects of external strains and fields, as well as on electron density variations induced by solvation, adsorbed molecules and ions, surface functional groups, *etc.*[26,102,109,149,150]

Calculations indicated that the WF of MoS_2 (and WS_2) depends on the number of layers, decreasing from 5.9 eV (5.7 eV for WS_2) for single layers to 5.6 eV (5.3 eV) for double-layer and to 5.4 eV (5.2 eV) for tri-layer formations of the same chemical composition.[96] We note that WF variations are discussed here in terms of absolute values relative to the vacuum level.

The work function of atomically thin phosphorene sheets was predicted to gradually decrease from *ca.* 5.2 eV down to *ca.* 4.5 eV as the number of layers was increased from 1 to 5.[151] Another spectacular example is antimonene which transforms from an indirect semiconductor as a single-layer to the metal as a bilayer.[25,71,73,102] Having extremely large surface-to-volume ratios, atomically thin 2D materials are very sensitive to the presence of defects and adatoms[102] as well as to external stimuli, showing strong and reversible changes of electronic properties under external electric fields[150,152,153] and strains.[74,102,149,150,154–156]

In ePV applications, a more practical way of tuning the electronic properties of 2D sheets is to modify them chemically, for example by the reduction/oxidation of the basal plane, adsorption of molecular species with different electron densities, introduction/modification of functional groups decorating the basal plane or adjusting the charge of the basal plane by interactions with ionic species.[26] These modifications can be introduced flexibly and at different stages, in particular, during the exfoliation of bulk precursors, in colloidal inks of 2D flakes, as well as after the film deposition.

4.1. Oxidation/reduction/doping of basal plane

Graphene oxide sheets decorated with numerous oxygen-containing functionalities (hydroxyls, carboxyls, epoxides, *etc.*) provide an excellent example of a broad WF tunability by chemical modifications of the basal plane.[26,35,76,100] The controlled reduction of GO can be performed by thermal annealing in a vacuum or by strong reducing agents such as hydrazine[76,100,101,157] as well as in a photochemical regime.[76,100,101,158] Thermal reduction of GO allows WF to be gradually decreased from 5.5 eV to 4.5 eV (Table 1). The WF correlates with the residual oxygen content indicating that the WF modifications originate from the elimination of oxygen-containing functionalities (Fig. 4a).[157]

The WF of single-layer MoS_2 can be increased from *ca.* 4.0 to 4.5 eV by controlled oxidation in a vacuum resembling the similar behavior of graphene.[180]

Thermal annealing of air-exposed polyheptazine carbon nitride ETLs results in gradual oxidation of the basal PCN plane and an increase of WF from 4.1 to 4.6 eV as the annealing temperature is elevated up to 250 °C.[93] The PCE of the PCN-based OSCs shows a volcano-shaped dependence on the annealing temperature (Fig. 4b), indicating there is an optimal ETL WF for the particular BHJ, that can be easily tuned for other donor/acceptor couples by the annealing parameters. The V_{oc} of PCN-based OSSs decreases linearly with a shift of absolute WF to higher values (Fig. 4b, insert), reflecting an increase in the recombination losses at the BHJ/ETL interface as the difference between the donor/acceptor highest occupied molecular orbital (HOMO) and ETL level becomes larger.[93] Deeper oxidation of PCN under UV/ozone treatment results in an even higher WF of *ca.* 5.3 eV, allowing PCN to be applied as HTL material in OSCs,[168] perfectly illustrating the variability of the charge-extraction capacity of atomically thin PCN.

Along with the above-discussed post-synthesis treatment of PCN sheets, a broad variety of modifications of the basal PCN plate can be performed during the polycondensation and formation of the polyheptazine network resulting in considerable changes in the electronic properties of final PCN sheets. These modifications include (i) substitution of native C or N atoms of the heptazine heterocycles or (ii) introducing additives in voids formed by adjacent heptazine units. By starting polycondensation from thiourea instead of conventional urea or

Table 1 Some of the reported variations of WF of atomically thin 2D materials

2D material	WF variation method	WF variation range	Ref.
Graphene	Intercalation/stacking	3.3–5.1	159
	Molecular doping	2.9–5.3	160
GO	Reduction	5.5–4.5	157
	Reduction/covalent functionalization	3.7–5.1	161
		4.9–5.2	162 and 163
	Covalent functionalization	4.8–5.0	164
	Deposition of Ag nanoparticles	4.9–4.7	165
	Neutralization with Li^+	4.9–4.0	163, 166 and 167
PCN	Oxidation	4.4–5.3	168
		4.1–4.6	93
Ti MXene	Oxidation/reduction	4.1–5.0	169
	Molecular doping	4.8–4.2	88
		4.2–5.0	170
		4.4–4.9	171
	Oxidation	4.7–5.4	172
		5.4–6.9	173
	Covalent functionalization	4.7–5.3	174
	Annealing	3.9–4.8	175

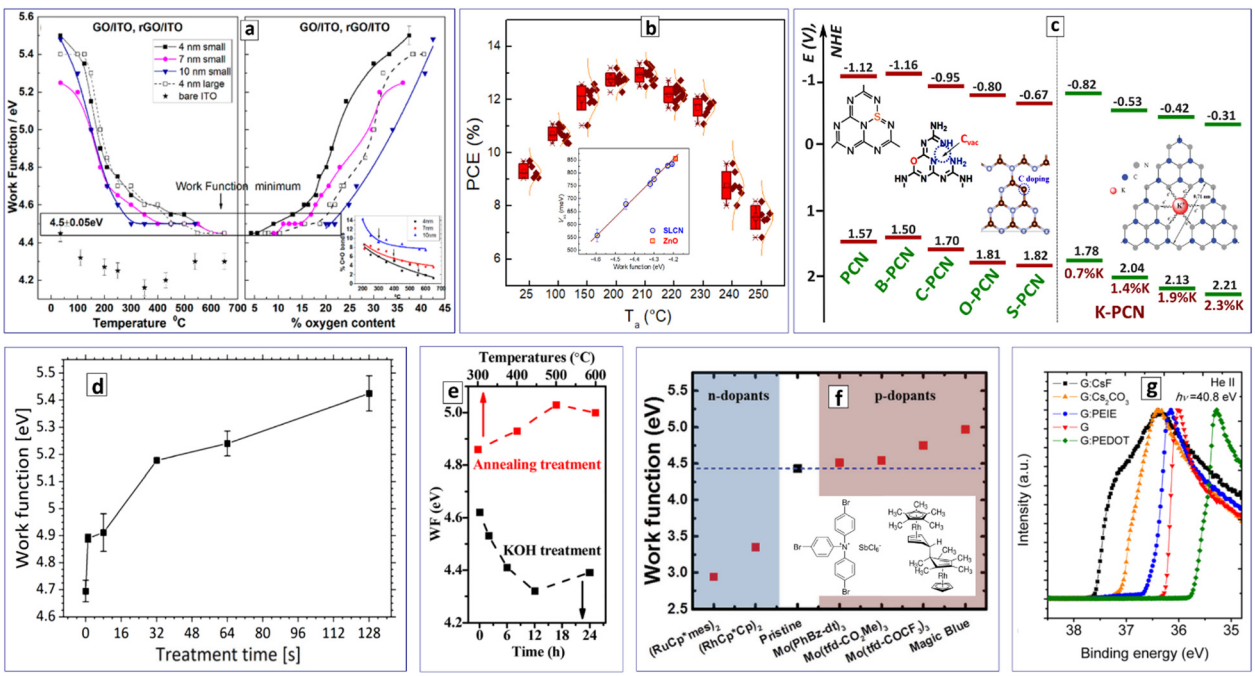

Fig. 4 Variations of WF of atomically thin 2D materials. (a) WF of GO as a function of vacuum-annealing temperature and oxygen content in GO. (b) PCE of a non-fullerene OSC with polyheptazine carbon nitride ETL as a function of ETL annealing temperature. Insert: dependence of V_{oc} on the ETL work function. More details are in ref. 93. (c) Band edge potentials of pristine and B-, C-, O-, and S-doped PCN (left section), and PCN doped with different amounts of K^+ (right section). The diagram was plotted using numerical data reported in ref. 65 and 176. Inserts show the proposed structures of some of the doped PCN samples. Potentials are presented *versus* normal hydrogen electrode (NHE). (d) The work function of $Ti_3C_2T_x$ MXene as a function of the duration of the oxygen-plasma treatment. (e) The work function of $Ti_3C_2T_x$ MXene as a function of the duration of thermal annealing and alkaline treatment. (f) The work function of graphene doped with different molecular species. Structures of Magic Blue and $(RuCp^*mes)_2$ are presented in the figure. (g) UV photoelectron spectra of graphene multi-layer stacks with different intercalates. See the description of abbreviations in ref. 162 (f) and ref. 164 (g). Reproduced with permissions from ref. 157 (a), ref. 176–179 (inserts in (c)), ref. 170 (d), ref. 83 (e), ref. 160 (f), and ref. 159 (g). Copyrights: (2015, 2016, 2021) American Chemical Society (a), (e) and (g); (2012, 2014, 2015, 2023) The Royal Society of Chemistry (inserts in (c) and (d)); (2017, 2021) Wiley-VCH GmbH (insert in (c) and (f)); (2022) Elsevier B.V. (insert in (c)).

melamine, a portion of native carbon atoms can be substituted with sulfur (Fig. 4c, inserts).[65,177] Polycondensation of supramolecular assemblies of melamine with cyanuric acid yields carbon-enriched (carbon-doped) PCN samples.[178] The introduction of formaldehyde during the polycondensation of molten urea yields oxygen-doped PCN with carbon vacancies,

forming spontaneously to retain the neutrality of the polyheptazine network.[179] Polycondensation of dicyandiamide in the presence of KOH gives ''2D-intercalated'' K-PCN products with K^+ localized in voids formed by adjacent heptazine units (see insert in Fig. 4c) that affect strongly the electron density distribution of PCN sheets.[176] All these modifications allow the position of the CB edge and, therefore, the Fermi level and WF of PCN to be varied by more than 0.8 eV (Fig. 4c). The PCN derivatives produced by doping and ''2D intercalation'' showed excellent photocatalytic activity, while their potential for PV applications is still to be evaluated.

Another example of the flexible charge extraction selectivity of 2D materials is provided by $Ti_3C_2T_x$ MXenes, which can be oxidized and reduced in a controlled way with their WF tuned for both ETL and HTL applications.[41,42,45,46,75,109,169,172,173,175] In particular, the WF of MXenes was varied between *ca.* 4 and 5 eV (Table 1) by UV/ozone oxidation and reduction with N_2H_4 yielding excellent HTL and ETL materials for non-fullerene OSCs with efficiencies comparable to conventional HTL/ETL materials.[169] Very fast and controllable oxidation of MXene layers at temperatures below 70 °C using high-power-density oxygen plasma (Fig. 4d) is very attractive for the production of OSCs on reactive flexible substrates.[172] Alternatively, $Ti_3C_2T_x$ MXenes can be oxidized directly in aqueous inks by mild thermal treatment, resulting in the conversion of Ti–C bonds into Ti–O bonds and the transition of the MXene from metallic to semiconducting state.[173] In this case, the WF can be tuned between *ca.* 5.4 and 6.9 eV by mixing oxidized and pristine MXenes and producing promising ETL materials for PSCs.[173]

4.2. Functionalization

Variations of WF through covalent and ionic functionalization were mostly demonstrated for GO[26,35,161–167] and MXenes,[41,42,45,46,75,83,88,109,110,132,170,171,174] both having abundant and versatile functional groups ready for substitution and coupling reactions.

Functionalizing graphene oxide with various fluorinated groups *via* nucleophilic substitution of native epoxy groups with piperidines yields atomically thin 2D materials with WF varied from 3.7 to 5.1 eV (Table 1).[161] A moderate WF variation (4.9–5.2 eV) was observed as a result of photochemical chlorination of GO.[162] This approach enables a very delicate WF tuning by varying the number of laser pulses GO films are subjected to.[162] Neutralization of carboxylate groups of photochlorinated GO with Li^+ decreases the WF back to 4.3 eV, allowing the pristine Cl–GO and neutralized Cl–GO–Li to be applied as efficient HTL and ETL materials in fullerene OSCs, respectively.[163,166] Additionally, Cl–GO–Li inter-layers between the absorber and titania ETL were found to protect OSCs from environmental humidity.[166] Similarly, GO (WF 4.7 eV) and Cs^+-neutralized GO (4.0 eV) can be used as HTL and ETL components of OSCs, respectively, outperforming reference cells with PEDOT:PSS HTLs and aluminum as ETL.[167] A WF decrease of GO sheets due to partial electron transfer to Ag nanoparticles deposited directly on GO sheets (Table 1) was used to fine-tune HTL for low-temperature-processed PSCs.[165]

Alkaline treatment of fluorinated Nb_2CT_x MXene sheets results in the substitution of –F groups with –OH groups, decreasing WF from *ca.* 4.6 to 4.3 eV, while further thermal annealing converts hydroxyls into =O groups resulting in a WF increase to *ca.* 5.0 eV (Fig. 4e).[83] In this way, both ETL and HTL materials for OSCs can be produced from the same atomically thin 2D precursor, showing superior charge-transport properties as compared to ZnO (ETL) and PEDOT:PSS (HTL) ref. 83. A similar approach was applied to tune the WF of $Ti_3C_2T_x$ MXenes yielding efficient titania/MXene ETLs for PSCs.[132]

Covalent grafting of $Ti_3C_2T_x$ MXenes with nitrophenyl groups results in an increase of the absolute WF between 4.7 and 5.3 eV (Table 1), proportional to the surface density of the anchored groups.[174] At the same time, the modification of the MXene with amino acids introduces surface dipoles reducing WF from 4.8 to 4.2 eV,[88] with a total WF variation ''window'' exceeding 1 eV if both methods are considered together. A similarly broad tuning of the WF of $Ti_3C_2T_x$ MXenes can be achieved by surface modification with ethanolamine reducing WF down to 4.2 eV, while the deposition of Rh nanoparticles increases WF up to *ca.* 5 eV. Both materials showed excellent electron- and hole-extracting properties in non-fullerene OSCs.[170]

Non-covalent interactions with molecular species with distinct electron-donating or electron-accepting properties were found to strongly influence the electron density distribution of atomically thin 2D materials, allowing their WF to be tuned in a large ''window'' of more than 2 eV (Table 1).[160,171,181–183] A perfect example of this approach is the WF evolution of a-few-layer graphene sheets upon interaction with strong reducing and oxidizing agents.[160] At that, the interaction of graphene with a strong acceptor – tris(4-bromophenyl)ammoniumyl hexachloroantimonate (Magic Blue) shifts WF from *ca.* 4.5 up to 5.0 eV, while the non-covalent doping with a strong donor – pentamethylrhodocene dimer decreases the WF of graphene to 2.9 eV (Fig. 4f).[160]

By introducing a series of molecular dopants with different redox properties as well as varying the dopant concentration, the WF of graphene can be smoothly tuned over the window of 2.9–5.0 eV yielding 2D materials with tailored charge extraction selectivity. This approach appeared to be universal allowing the broad WF tuning of other atomically thin 2D materials, including TMDCs[181–183] and MXenes.[171] In the latter case, the noncovalent-dopant-controlled WF variation is especially attractive because it can be performed without affecting the type and density of functional groups.[171]

4.3. Intercalation

As we discuss in Section 6, the spontaneous formation of self-assembled multi-layer stacks and intercalates from single-layer 2D materials is a highly promising route to new PV-relevant materials with tailored electronic characteristics. This tunability is exemplified by WF variations reported for graphene intercalates produced by stacking the single-layer graphene sheets in aqueous solutions of intercalating agents.[26,159] Depending on the type of intercalated species, such multilayer films showed WF varying from *ca.* 3.3 eV for intercalated

CsF up to 5.1 eV for intercalated PEDOT molecules (Fig. 4g), providing an almost 2-eV window of WF variation. The intercalates were manufactured using low-temperature solution chemistry from graphene grown by chemical vapor deposition and applied as ETL and HTL of fullerene OSCs.[159]

5. Solution-processing of 2DM inks for printed ePV

Mechanical exfoliation of layered bulk materials is probably the most straightforward approach to corresponding atomically thin 2D derivatives.[21,26,28–30,36,52,67,71,73,103,105] This approach was pioneered to produce micron-size single-layer graphene[20,26,28–30,44] and afterward applied to different layered solids, such as MoS_2,[49,50,52,53,67,69,115,184] antimony,[25,70,71,73,102] BP,[36,103,105] and other 2DMs. The mechanical exfoliation is, though, hardly scalable for mass production of 2D materials and requires the tedious transfer of 2D flakes from adhesive tapes to target substrates. Although mechanical exfoliation was recently shown to be upscalable to the roll-to-roll production of large-area 2DM films, the final products are typically multilayer sheets with a thickness of 10–100 nm.[185]

Various types of epitaxial growth, such as molecular beam epitaxy, chemical (physical) vapor deposition (CVD/PVD), or atomic layer deposition (ALD) provide excellent control over the thickness and stoichiometry of the 2D materials but also typically require post-synthesis inter-substrate transfer.[25,70]

In contrast to those methods, liquid-phase exfoliation (LPE) of layered 2D solids was recognized as a versatile, relatively ''green'' and cost-effective approach allowing the production of atomically thin 2DMs to be upscaled to the industrial level. This approach can yield stable liquid inks ready for ''wet'' film deposition, in particular, by printing technologies, at the same time ensuring reliable control over the morphology and properties of 2DM flakes.[21,24–28,33,36,41–46,55,56,63,64,69–75,102–105,184,186] The development of LPE-based approaches to the colloidal 2DM inks was considerably stimulated by the transition from high-temperature-processed mesoscopic metal-oxide charge transport layers in PSCs to planar metal-oxide charge-collecting layers deposited and processed at low temperatures.[24,28,30,33] At that, LPE can be realized in a plethora of versions, including spontaneous, intercalation-assisted, mechanochemical, and electrochemical exfoliation.[21,24,56,63]

The liquid ''inks'' of exfoliated 2DMs can then be processed using a variety of established solution-based processing techniques, including spin/dip/spray coatings and inkjet printing.[56,63,187] Recently, remarkable progress was achieved in the development of scalable and sustainable technologies for the mass production of 2DM films, highlighting spray coating, inkjet printing, and extrusion-based 3D printing as the most promising venues.[187] These technologies allow 2DMs to be deposited with high precision and complement each other. The spray coating is suitable for the production of large-area films with controlled thickness and roughness. The inkjet printing is focused on smaller and more sophisticated patterns. The extrusion-based printing yields robust and shape-conserving 3D architectures. At that, all these approaches show a large room for upscaling and automation.[187]

One of the best examples of spontaneous LPE was provided by graphene, showing the feasibility of room-temperature exfoliation of graphite into 2D flakes in solvents with appropriate solvation energy compensating the interlayer bonding energy.[21,44,134,188,189] For example, imidazolium-based ionic liquids with tailored surface tension are capable of exfoliating graphite spontaneously at room temperature.[190] The interaction of graphite with ionic liquids can be strongly accelerated by microwave irradiation resulting in spectacularly fast LPE with high yields and selectivity for the atomically thin graphene sheets. The exfoliated product can be converted into concentrated inks (*ca.* 100 mg mL^{-1}) with 95% of sheets showing a thickness below 1 nm (Fig. 5a) and negligible structural deterioration.[191] Stable and concentrated graphene inks were also produced by the LPE of graphite in chlorosulfonic acid.[192,193] The exfoliation rate and stability of final graphene inks can be increased by adding stabilizers, such as thiourea.[89]

Similar to graphene, single-layer antimonene was produced from pulverized Sb powder by ultrasound-assisted exfoliation in butanol.[25,71,92,102] Imidazolium-based ionic liquids electrostatically stabilize exfoliated antimonene sheets yielding inks with two orders of magnitude higher concentrations.[118,140,147]

Atomically thin phosphorene sheets were produced by spontaneous BP exfoliation by sheer stress induced by a combination of centrifugal and gravitational forces created in a rapidly rotated vortex fluidic device. Simultaneous illumination of the vessel by near-infrared laser imparts the sheets with high vibrational energy and overrides the inter-layer van-der-Waals forces.[81] This approach shortens the exfoliation time by an order of magnitude yielding stable and processable phosphorene inks in 2-propanol.

Liquid-phase exfoliation of graphite and other layered bulk materials is typically accelerated by ultrasonic irradiation which facilitates the penetration of solvent in the interlayer galleries and, at the same time, fractures the bulk materials into smaller pieces, making them more accessible to intercalation.[55,56,199] Alternative to ultrasonication, colloidal 2DM inks can be produced using a wet-jet milling process, where suspension of a bulk layered precursor is forwarded under high pressure (180–250 MPa) through a system of perforated disks with holes of different diameters generating shear forces and resulting in the spontaneous exfoliation.[63,199] This method offers an unprecedented productivity of more than 2 L per hour of stable 2DM inks with a concentration of *ca.* 10 g L^{-1} and can be applied to various layered materials, including graphite, boron nitride, and TMDCs.[63,199]

Spontaneous ultrasound-assisted exfoliation of graphite oxide yields single-layer GO which can then be converted into reduced graphene oxide (RGO) with aromaticity tuned by thermal,[95,139,157] chemical,[78,95,157,161] or photochemical[100,158,162] reduction. Layered graphite oxide is typically synthesized *via* oxidizing graphite to graphite oxide with a mixture of concentrated H_2SO_4, $NaNO_3$, and $KMnO_4$, followed by

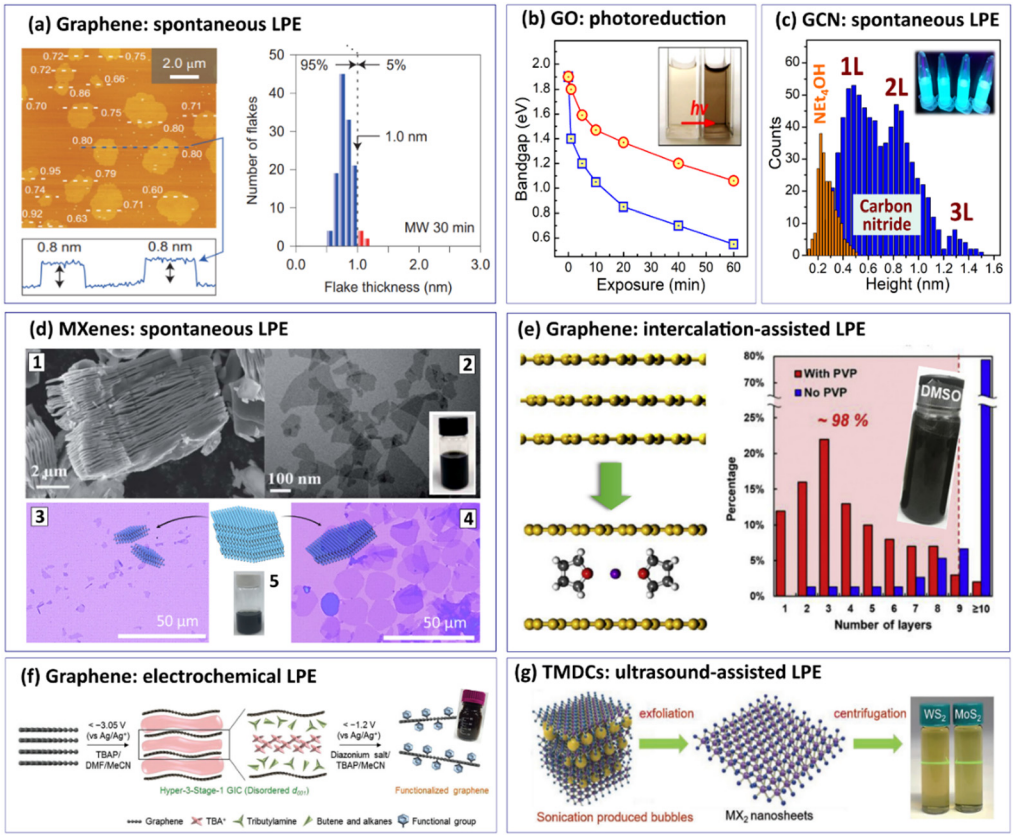

Fig. 5 (a) AFM image (left panel) and thickness distribution (right panel) of graphene sheets in an ink produced by spontaneous LPE exfoliation of graphite in an ionic liquid. (b) Bandgap evolution during photoreduction of colloidal GO in pure water (circles) and aqueous N_2H_4 solution (squares); Insert shows photographs of original and photoreduced GO; (c) thickness distribution of PCN sheets exfoliated in aqueous NEt_4OH solutions; insert shows exemplary photographs of colloidal SLCN under UV illumination (more detail in ref. 194 and 195); (d) SEM photographs (1–4) of non-exfoliated MXene (1) and ultrasonic exfoliation products (2), vigorous shaking (3), and mild shaking (4); photograph of a typical MXene ink (5). (e) Scheme of graphene intercalation, flake thickness distribution in graphene ink, and a photograph of the ink (3); (f) scheme of electrochemical LPE/covalent functionalization of graphene sheets; (g) scheme of ultrasound-assisted exfoliation of TMDCs and photographs of resulting MoS_2 and WS_2 inks. Reproduced with permissions from ref. 191 (a), ref. 87 ((d), cases 1 and 2), ref. 196 ((d), cases 3–5), ref. 197 (e), ref. 198 (f), and ref. 96 (g). Copyrights: (2015) Springer Nature Ltd. (a); (2019) The Royal Society of Chemistry ((d), cases 1 and 2); (2022) American Chemical Society ((d), cases 3–5); (2018) Elsevier Ltd. (e); (2017) Wiley-VCH GmbH (f) and (g).

ultrasound-assisted exfoliation into colloidal GO in water.[76,78,80,90,94,95,100,101,138,157,161,162,166] Stable and processable GO inks can be produced by ultrasonic treatment in polar water/dimethylformamide (DFM) mixtures.[139]

Reduction of GO results in the elimination of oxygen-containing functionalities (carboxyl, epoxy, hydroxyl, *etc.*) and gradual restoration of the aromatic character of the basal plane.[76,100,101] In cases of chemical reduction, these transformations are often accompanied by grafting of the basal plane with various functional groups (fluorinated alkyls[161] and aryls,[78] silanes,[164] OSO_3H,[94] derivatives of piperidine and piperazine[161]), modifying the electronic properties of RGO[76,101] and making it dispersable in various solvents (chloroform, chlorobenzenes, toluene, DMF, ethylene glycol[78,161,164]), suitable for solution-processed ePV. Photochemical reduction of GO is an attractive approach,[76,100,158] as it can be performed in mild conditions both for inks and films, allowing the bandgap, WF, and conductivity of RGO to be reliably controlled by varying light exposure and introducing additional reductants (Fig. 5b). Parallel photochemical reactions can be performed to further modify RGO, for example, photochlorination of the basal plane.[162]

The solubility of RGO in water decreases rapidly as the reduction depth increases due to the elimination of functionalities.[91,200] In this situation, stable aqueous inks can be produced by stabilizing RGO with colloidal GO,[91] most probably *via* the formation of van-der-Waals aggregates.

Ultrasound-assisted exfoliation of bulk polyheptazine graphitic carbon nitride (GCN) typically results in partial delamination and formation of multi-layer GCN flakes regardless of the used solvent.[55,129,133,141,142,168] The spontaneous exfoliation of bulk GCN down to single-layer polyheptazines was reported in aqueous concentrated NaOH solutions, most probably due to nucleophilic substitution of residual NH_2 groups with OH, imparting CN layers with a negative charge and facilitating the delamination.[201] A-few-layer flakes of GCN were produced by ultrasound-assisted delamination in 1,3-butanediol.[202]

Thermal etching of bulk GCN on air was reported to disrupt interlayer bonding and drive the ultrasound-assisted exfoliation toward the formation of single-layer and double-layer CN inks.[203–206]

Bulk GCN was found to exfoliate spontaneously in hot aqueous solutions of tetraethylammonium hydroxide (NEt_4OH) yielding stable optical transparent polyheptazine inks with a nominal C_3N_4 concentration over 0.5 M. The majority of exfoliated flakes have thicknesses of *ca.* 0.5 and 0.9 nm, corresponding to single-layer and double-layer polyheptazine sheets (Fig. 5c).[194,195,207,208] The colloidal PCN inks show a bulk-like bandgap of *ca.* 2.7 eV and intense photoluminescence (PL) with a PL quantum yield (QYs) of *ca.* 50% (Fig. 5c, insert), indicative of a low charge trap density. Liquid inks with atomically thin polyheptazine sheets can be produced by modifying the GCN structure with exo-templates.[195] For example, the polycondensation of urea intercalated in the galleries of layered double hydroxides yields single-layer carbon nitride confined between neighboring layers of the host.[125] Acidic etching of the template yields PCN sheets with a thickness below 1 nm, forming stable inks DMF.

A polymorph of GCN, polytriazineimide, shows lower energy of interlayer van-der-Waals interaction and exfoliates spontaneously into atomically thin sheets in aprotic polar solvents, such as dimethylsulfoxide (DMSO) and DMF avoiding possible damage of the layers by the ultrasonic treatment.[130]

Bulk molybdenum disulfide was exfoliated into 3–4 nm thick flakes by mild ultrasonic treatment of bulk material in a hot water/ethanol bath.[209] By increasing the power of ultrasonic irradiation the cavitation effect can be achieved in water/ethanol[96] and water/ammonia mixtures,[146] generating bubbles that penetrate between the MoS_2 and WS_2 layers enhancing the exfoliation into atomically thin flakes.

Layered MXenes, for example, $Ti_3C_2T_x$ or Nb_2CT_x show a pronounced trend to spontaneous exfoliation into single-layer MXenes under ultrasonic irradiation[46,75,83,85,87,88,121,122,128,132,135,136,169] as well as in much milder conditions of manual shaking.[79,143,196] The aluminum etching in the precursor MAX phase can also be performed in relatively mild conditions by contacting Ti_3AlC_2 with a mixture of LiF and concentrated HCl, or with $ZnCl_2$,[148] yielding MXenes with T = F or Cl, respectively.

The lateral size of MXene flakes depends strongly on the conditions of the exfoliation (Fig. 5d), increasing from 1–3 μm for standard sonication[137] to 2–10 μm for continuous manual shaking[143,196] and even up to 40 μm under minimal stirring of the exfoliating MXene sheets.[79,196] A similar methodology was also applied to produce liquid inks of other MXene compounds, in particular, Ti_3CNT_x[143] and Nb_2CT_x.[83] Alternatively, the lateral size of MXene sheets can be reduced to a few nanometers by subjecting lamellar $Ti_3C_2T_x$ suspended in ethyl acetate to ultrasonication and pulsed laser illumination.[127]

5.1. Intercalation-assisted LPE

Graphite is well known for its rich chemistry of intercalated compounds,[56,210] many serving as natural precursors for spontaneous LPE. In particular, stage-1 intercalates of potassium-tetrahydrofuran (THF) spontaneously delaminate upon contact with DMSO. Introduction of polyvinyl pyrrolidone stabilizes inks with atomically thin graphene sheets with layer number below 10 (Fig. 5e).[197] Upon ultrasonic treatment graphite can be oxidized and simultaneously intercalated with a mixture of concentrated H_2SO_4 and HNO_3 yielding colloidal nanosheets of a-few-layer graphite.[211]

Molybdenum and tungsten sulfides intercalated with Li^+ were reported to spontaneously exfoliate in water to atomically thin sheets consisting of 2–3 monolayers.[184,212,213]

Colloidal a-few-layer bismuthene sheets were produced by the exfoliation of H_2SO_4-intercalated bulk Bi. The exfoliation is facilitated by the introduction of ammonium persulfate and H_2O_2. The former oxidizes the edges of the Bi sheets, while the latter generates oxygen bubbles and expands the layered bulk material.[97,214] In a similar way, the formation of gaseous SbH_3 during hydrolysis of a Li_3Sb alloy produced by lithiation of antimony with butyllithium assists the alloy exfoliation into colloidal single-layer Sb sheets.[77]

Interaction of GCN with concentrated H_2SO_4 simultaneously results in the partial oxidation of single polyheptazine layers, intercalation of acid, and the grafting of carboxyl groups into PCN sheets. Both the intercalation and functionalization facilitate the delamination of the intercalated GCN into single-layer sheets at subsequent ultrasonic treatment.[55,213,215] Supercritical treatment of GCN with ammonia results in the intercalation of NH_3 molecules between the layers and total delamination to single-layer sheets during the following ultrasound treatment.[216]

Mechanochemical exfoliation of bulk layered materials is achieved by mechanical grinding of the precursors in a planetary mill filled by colliding hard inert balls, resulting in the formation of a-few-layer flakes.[217,218] The re-stacking can be prevented by introducing stabilizing additives and/or solvents as well as by partial oxidation under massive mechanical stress, resulting in the functionalization of the 2DM surface.[217,218] In the former case, the ball-milling can directly yield liquid inks, while the latter treatment is typically followed by spontaneous or ultrasonically-assisted dispersion. Though being universal and potentially upscalable to industrial production levels, the mechanochemical exfoliation typically yields relatively thick sheets consisting of 10 or more layers, thus requiring additional exfoliation by other approaches to reach the single-layer/a-few-layer state of the final 2DMs.

Within this approach, BP sheets with 7–15 single layers were produced by ball-milling of the bulk precursor in a low-melting-point medium (urea–glucose–NH_4Cl) followed by the dispersion in organic solvents.[219] Mechanochemical exfoliation of graphite[220] or MoS_2[221,222] can be achieved in the presence of NaCl as a "hard" additive results in a-few-layer products readily dispersible in organic solvents, such as *N*-methyl pyrrolidone, DMF, or ethanol. Introducing both graphite and MoS_2 2D heterostructures can be directly produced with high yields (*ca.* 75%).[221] Mechanochemical treatment of graphite with $KMnO_4/H_2SO_4$ allows exfoliation to be combined with graphite oxidation into graphite oxide, further exfoliating into GO under ultrasonic treatment in water.[223,224] Solvent-free

mechanochemical exfoliation of MoS_2 to one-two-layer sheets was achieved with yields higher than 60% in the presence of graphene nanosheets as a stabilizer.[225] A broad variety of MXenes was produced by mechanochemical approaches.[218]

Recently, the grinding exfoliation was introduced as an industrially-upscalable version of the mechanochemical treatment, where mixtures of layered materials and hard microcrystalline additives are ground under a circularly moving press with the additives playing the role of milling balls and forcing the exfoliation of the layered precursor.[226,227] This approach was developed for mixtures of MoS_2 and Mo_2C as a hard additive[226] and further extended to other 2DMs such as boron nitride, BP, and TMDCs, producing and water-dispersible sheets composed of 10–15 layers with high yields (60–70%).[227]

Electrochemical exfoliation is an elegant and scalable approach to the delamination of layered bulk materials into single-layer and a-few-layer fragments by electrically driven intercalation and oxidation phenomena.[21,25,56,75,109,112,137,184,228–230] Typically, it is performed in a two-electrode cell with bulk materials as one of the electrodes. The electrolyte usually contains bulky cations capable of bias-driven intercalation between the layers of the exfoliated bulk material.

In particular, electrochemically intercalation of tetrabutyl (TBA) cations in graphite yields hyperstage-1 intercalates with an interlayer distance exceeding 1.5 nm.[198] These intercalates react with diazonium salts resulting in spontaneous exfoliation and decoration of graphene sheets with 3,5-dinitrophenyl groups providing excellent dispersibility in DMF.[198] A-few-layer phosphorene sheets were produced by one-step electrochemical exfoliation of BP in the presence of TBA salts.[137] At that, $TBABF_4$ electrolyte supplies fluoride anions that can be oxidized on the counter electrode and react with exfoliated flakes yielding fluorinated phosphorene.[137] The BP-TBA intercalate can be exfoliated into stable a-few-layer phosphorene inks *via* a mild ultrasonic treatment in DMSO.[86] Electrochemical etching of MAX phases allows $Ti_3C_2T_x$ sheets to be produced in mild HF-free and controlled conditions.[111,112]

6. Self-assembly of 2DMs

The solution-based synthetic approaches to atomically thin 2DMs are focused on the exfoliation of layered bulk precursors with the colloidal 2D sheets typically decorated with functional groups or ligands preventing their immediate re-stacking. Destabilization of 2DM colloids, for example, by compensating surface charge or by eliminating solvent/ligands, results in the self-assembly of the atomically thin colloidal sheets into layered aggregates bound by Van-der-Waals (VdW) interactions, often capturing intercalated compounds from the original ink.[21,231–233] This capability to self-organize opens a tremendous potential for a combinatorial design of new composite materials, combining different 2D species and functional additives captured in the inter-layer galleries of such VdW assemblies.[17,18,20,21,24,48,58,62,68,99,104,231–236] The self-assembled materials reveal atomically abrupt changes of properties on the interfaces between 2D components avoiding the formation of dangling bonds and defects typical for the covalently bound heterojunctions.[24] At that, the existing ''library'' of single-layer and atomically-thin 2DMs can be used as a sort of a ''Lego'' set to construct a variety of new materials by alternatively stacking identical and different layers on top of each other (Fig. 6a).[234]

The liquid-phase exfoliation of layered materials is very often driven by surface oxidation of bulk precursors and electrostatic repulsion between newly-formed ionized functional groups of neighboring monolayers. In this situation, the edges of exfoliated 2D sheets are enriched with functionalities that can interact with edge functionalities of other sheets resulting in two-dimensional (''horizontal'') self-assembly of 2D sheets into larger-area thin films.[58,68,236] This tendency can be used to spontaneously form macroscopic conductive/semiconductive films serving as efficient charge-transport layers in PV cells and still retaining atomically-thin character. An example is provided by $Ti_3C_2T_x$ MXene forming large-area single-layer self-assemblies on the surface of silicon, showing extremely low resistivities and highly efficient electron-collecting behavior.[240]

A much more frequently observed and exploited self-assembly mode is the spontaneous VdW stacking of atomically thin 2D sheets into multi-layer formations.[21,24,58,62,68,99,232,233,236,241] For example, single-layer graphene sheets introduced into aqueous solutions show a tendency to restack and form intercalates of dissolved compounds.[159,232,236] The intercalation allows the WF of the self-assembled graphene films to be varied in a broad range (see Section 4) covering potential applications as both ETL and HTL components and showing high conductivities already for 2–3 graphene layers (Fig. 6b).[159]

Slow evaporation of water from single-layer PCN inks results in spontaneous self-assembly of PCN sheets into loosely aggregated multi-layered formation with an interlayer distance almost twice as large as for the original bulk PCN (Fig. 6c) due to the intercalation of stabilizing NEt_4OH additive.[207,208] Simultaneously with the vertical stacking, the single-layer PCN shows a tendency for horizontal self-assembly into honeycomb-shaped frameworks with walls formed by 2–3 layers of PCN (Fig. 6d).[207,208] Such self-assembled films revealed excellent electron-transport properties in non-fullerene OSCs.[93]

Vertical stacks of atomically thin sheets can be produced by solution-processable layer-by-layer electrostatic assembly, exemplified by electrostatic GO self-assemblies with polydiallyldimethylammonium (PDDA) chloride.[242] In this approach, a substrate is alternatively immersed into an aqueous ink of negatively charged GO sheets and a solution of positively charged polyelectrolyte macro-molecules, forming self-assembled stacks with easily controlled thickness. Despite the presence of PDDA between GO layers, the assemblies are competitive to PEDOT:PSS as an HTL material for OSCs, with the best performance observed for the films with 2 GO layers.[242]

The tendency of atomically thin 2DMs to vertical VdW self-assembly reveals an immense potential for the synthesis of new composite materials by stacking different 2D sheets into the so-called Janus assemblies.[20,21,24,48,52,53,58,62,68,99,104,231–234,236,241]

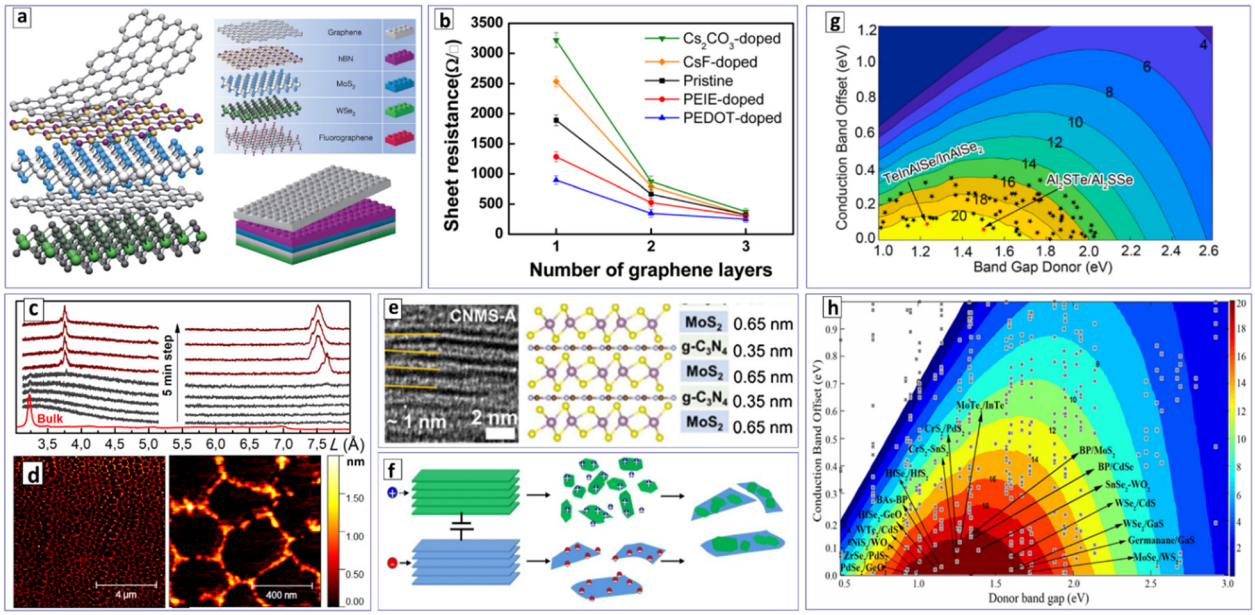

Fig. 6 Self-assemblies of atomically-thin 2DMs. (a) Schematic building of van-der-Waals heterostructures from a library of single-layer 2DMs similar to "Lego"-like constructions. (b) The sheet resistance of self-assembled graphene intercalates as a function of graphene layer number. (c) Temporal evolution of XRD pattern of single-layer PCN ink during spontaneous solvent evaporation. (d) AFM images of self-assembled PCN film on atomically smooth mica. More details on (c) and (d) can be found in ref. 207 and 208. (e) TEM image and schematic structure of PCN/MoS_2 self-assemblies. (f) Scheme of electrochemical exfoliation-assisted formation of bi-layer Janus heterostructures. (g) and (h) Calculated PCE as a function of donor bandgap and conduction band offset in various Janus bilayer heterostructures. Reproduced with permissions from ref. 234 (a), ref. 159 (b), ref. 213 (e), ref. 237 (f), ref. 238 (g), and ref. 239 (h). Copyrights: (2013) Macmillan Publishers Limited (a); (2015, 2018, 2022) American Chemical Society (b), (g) and (h); (2020) Elsevier B.V. (e); (2023) Wiley-VCH GmbH (f).

The stacking is typically performed for two single-layer components, one having a positive surface charge, and another – a negative surface charge, allowing perfect control over the electrostatic assembly in solution-based processing.[21,232,236] This approach is illustrated by alternating self-assembly of single-layer PCN and MoS_2 sheets, showing zeta potential of +32 mV and −35 mV, respectively.[213] By consecutively immersing a substrate into PCN and MoS_2 inks, interstratified composites can be produced with alternating PCN and MoS_2 single-layers and a superlattice period of *ca.* 1 nm (Fig. 6e). The PCN/MoS_2 self-assembly showed high photo- and electrocatalytic activity, making it potentially promising for PV applications as well.[213] Binary $ZnIn_2S_4$/$MoSe_2$ heterostructure produced by electrostatic self-assembly showed prominent photocatalytic activity in water reduction to H_2 due to highly efficient charge separation between the atomically thin components.[243]

Electrochemical LPE of two different layered materials on cathode and anode yields simultaneously negatively and positively changed 2D sheets (Fig. 6f), ready for further electrostatic self-assembly into Janus heterostructures.[237] The general applicability of this approach was proven for a variety of materials, including graphene and TMDCs.[232]

The properties of bi-component Janus heterostructures can be broadly tailored, both by varying the composition of components and the character of stacking. Still, the cases of practical applications of such composites in light-harvesting applications, in particular, emerging PV, are rather rare. Along with the above-discussed examples, only a few more can be found, including the application of VdW assemblies of pristine and oxidized $Ti_3C_2T_x$ MXenes as efficient ETLs in PSCs[173] and graphene/MAPI/graphene stacks in prototype photodetectors.[244]

At the same time, the potential for combinatorial synthesis of Janus hetero-stacks is immense, potentially including thousands of possible combinations.[21,68,233] Considering this complexity, the search for new ePV-relevant materials and targeted selection of the most promising combinations can be strongly supported by high-throughput (HTP) computational screening of monolayer materials and their stacking assemblies, which has been rapidly developing in recent years, encompassing not only ePV but also catalytic, ferromagnetic, piezoelectric and other materials.[245,246]

The HTP computational screening focuses on different aspects of the pipeline leading from the original bulk layered materials[247–250] to exfoliated monolayers[251] to bilayer[252] and Janus[238,253,254] combinations of single-layer materials to final optoelectronic devices.[238,239]

The HTP computational estimation of the exfoliation feasibility was performed starting from a large database of *ca.* 100 000 bulk compounds identifying *ca.* 2000 potentially exfoliable materials.[249] In a later report, the exfoliability of more than 10 000 layered compounds was evaluated based on the first-principles calculated elasticity tensor.[248] A dedicated computational study of MXenes identified 136 potentially exfoliable bulk MAX compounds that can be converted into 26 MXenes.[247]

An HTP computational screening of *ca.* 1000 monolayer semiconductors allowed many parameters of such materials, such as lattice constants, formation energy, Young's modulus, Poisson's ratio, shear modulus, anisotropic effective mass, band structure, band gap, ionization energy, electron affinity, to be calculated and assembled in a database.[251]

The search for exotic quantum states and properties often observed for bilayer semiconductors requires browsing a vast combinatorial space with different stacking models.[252,255] Very recently reported HTP density functional theory (DFT) calculations of binding energies of *ca.* 8500 homo-bilayer structures produced by stacking of 1052 monolayers in different configurations can accelerate this search drastically.[252,255] In particular, these computations identified more than 120 bilayer compounds with direct bandgaps produced from monolayers originally having indirect bandgaps.[252]

A computational DFT screening of *ca.* 20 000 Janus Van-der-Waals heterostructures identified *ca.* 70 potential candidates as ePV absorbers capable of reaching power conversion efficiencies beyond 20% (Fig. 6g).[238] A recent HTP DFT screening of Schottky junctions formed by metallic and semiconductor TMDC monolayers with a wide range of bandgaps and WFs resulted in a database available for the design of new ePV-relevant materials.[253] Computational screening of Janus bilayer structures of graphene with TMDCs indicated the formation of an in-built electrical field enabling charge separation between the components on the femtosecond time scale.[254]

A set of more than 1500 stack heterostructures formed from a library of 56 monolayer components was tested by HTP DFT calculations for potential applications as excitonic absorbers in ePV cells, identifying more than 90 composites with PCE beyond 15% and 17 best candidates with PCE exceeding 20% (Fig. 6h).[239]

To enable the development of machine learning (ML)-assisted HTP material screening and application of artificial intelligence, several computational databases were collected and published.[250,253,256] For example, a computational database of *ca.* 6000 monolayer compounds (2DMatPedia) derived from existing materials by substituting elements with analogs from the same group of the periodic table was introduced.[245,250] A computational database of pristine and defect monolayer 2D materials (2D Material Defect) was recently presented[260] with defect states in phosphorene, MoS_2, BN, InSe, and other monolayer materials calculated using HTP DFT as a potential basis for training of ML algorithms.

7. Conclusion and outlook

Atomically thin 2D materials, such as graphene and graphene oxide, covalent organic frameworks, layered carbides, and metal dichalcogenides, reveal a unique combination of properties, ensuring their prospects and applicability in energy generation, conversion, and storage, including light harvesting in emerging PV devices. With the major portion of the atoms on the surface, the 2DMs allow a broad variability of the bandgap and interband transition type, charge carrier mobility, Fermi level and work function, *etc.*, *via* relatively mild chemical modifications, application of external stimuli, or combination with other 2D species into van-der-Waals heterostructures. This flexibility of electronic properties marks 2DMs as universal charge transport components in ePV cells, capable of acting both as ETL or HTL materials with flexibly tailorable energy levels, hydrophilicity, and compatibility with other components of ePV devices.

The solution-based processing of 2DMs, while posing certain challenges in terms of quality, purity, and morphological control of final inks, has a large potential for industrial upscalability which can be a decisive contributor to the future progress of ePV technologies. The approaches of liquid-phase exfoliation are readily upscalable and can be automatized, as highlighted by the exemplary case of the wet-jet milling process, capable of the high-throughout and continuous production of numerous 2DMs in the form of concentrated liquid inks ready for further printing applications. The mechano- and electrochemically-driven LPE is expected to have a large upscalability potential, allowing the exfoliation of bulk layered precursors to be combined with chemical modification, highly controlled WF variation, and spontaneous *in situ* self-assembly of 2DMs.

The broad variability of the work function is a characteristic ''trademark'' of 2DMs that can become a game changer in the selection of charge transport materials, conventionally treated as ''static'' components with strictly defined energy levels. By using 2DM ETLs and HTLs with variable work functions, the energy levels of all cell components can be flexibly tuned and adapted to specific ePV absorbers, providing two additional variables for the experimental and computational optimization of the charge generation and flows in ePV devices. At that, variations in the energy level arrangement will be accompanied by minimal changes in the structure and manufacturing of the ePV cell, because WF tuning can be performed with minimized and/or well-controlled chemical changes of the charge transport components. This opportunity reveals a strong contrast to the current state-of-the-art when WF values of ETL/HTL components can only be changed by introducing new contact materials requiring substantial modifications of the cell manufacturing protocols and bringing risks of cell instability and unwanted side reactions with absorbers and other cell components. In the case of 2D contact materials, the cell manufacturing can be adapted for specific ETL/HTL combinations, for example, MXene ETL and GO HTL, and this particular ETL/HTL couple can then be subjected to broad WF variations for both contact materials easily performed within the same device manufacturing routine.

The flexibility of electronic properties of atomically thin 2DMs comes along with their rather unique convertibility into liquid inks ready for solution-based processing of ePV devices using various printing technologies. This combination of tunable properties and ''wet'' processability opens broad perspectives for the integration of 2DMs as light-harvesting and charge-transporting components in low-temperature-processed printable ePV on reactive or flexible substrates.

Along with being competitive with conventional ETL/HTL materials and having the WF variability as a unique ''selling point'', atomically thin contact materials can bring additional benefits to ePV devices based on disordered semiconductors, in particular lead-halide perovskites. The deposition of perovskites on 2DM supports was convincingly shown to yield more uniform absorber films with larger grains, passivated grain boundaries and suppressed surface recombination. The passivating role of 2DMs, both in charge transport layers and as additives to the active layer, can be further extended and used to suppress ionic transport and bind loose Pb^{2+} forming as one of the degradation products, suppressing potential lead release during the outdoor exploitation of perovskite solar modules. At the same time, many 2DMs, such as MXenes and GO showed pronounced shielding effects against environmental moisture resulting in spectacular examples of stable ePV devices already upscaled to the level of minimodules.

With variable work function, high conductivity, and a broad range of spectral transparency, 2DMs can be considered promising interface materials for tandem and more complex multi-junction ePV solar cells. For this prospective application, wide-bandgap 2DMs, such as GO, PCN, or phosphorene, are of special interest. A combination of tailored 2DMs such as ETL, HTL, and interface components can become a viable route for flexible multi-junction solar cells.

Along with the broad variations of the work function, the atomically thin 2DMs offer another unique opportunity for materials design *via* combinatorial stacking of the same and different single and a-few-layer formations into vertical van-der-Waals assemblies. The library of ''building blocks'' is already large, including graphene and RGO in various reduction depths, Xene sheets, covalent frameworks, such as PCN and PTI, tens of MXenes, and TMDC sheets, and is growing continuously. Considering the straightforward rules of layer-by-layer electrostatically driven self-assembly and the possibility of alternating 2D sheets with oppositely charged small and polymeric ions, the number of potential heterostructures becomes enormous and limited only by the imagination and resources of the experimenter.

This vast compositional field offers perfect opportunities for computation-driven accelerated discovery of new materials with targeted properties, such as charge separation and transport, mechanical flexibility, and optical responses. The progress in van-der-Waals assemblies of atomically thin 2DMs as functional and tunable components of ePV devices is expected to be closely related to and strongly boosted by the development of machine-learning-based methodologies of high-throughput material screening and accelerated optimization of single- and multi-junction ePV solar cells.

Author contributions

O. Stroyuk: conceptualization (lead), writing – original draft preparation (lead); O. Raievska: conceptualization (equal), writing – review & editing (equal); J. Hauch: conceptualization (equal), project administration (lead), writing – review & editing (equal); C. J. Brabec: conceptualization (equal), funding acquisition (lead), writing – review & editing (equal).

Data availability

No primary research results, software or code have been included and no new data were generated or analysed as part of this review.

Conflicts of interest

There are no conflicts to declare.

Notes and references

1 M. Victoria, N. Haegel, I. M. Peters, R. Sinton, A. Jäger-Waldau, C. del Cañizo, C. Breyer, M. Stocks, A. Blakers, I. Kaizuka, K. Komoto and A. Smets, *Joule*, 2021, **5**, 1041.
2 I. Kougias, N. Taylor, G. Kakoulaki and A. Jäger-Waldau, *Renewable Sustainable Energy Rev.*, 2021, **144**, 111017.
3 S. Lin, T. Zhang, H. Yang and Y. Li, *Energy Fuels*, 2024, **38**, 761.
4 C. Breyer, D. Bogdanov, M. Ram, S. Khalili, E. Vartiainen, D. Moser, E. R. Medina, G. Masson, A. Aghahosseini, T. N. O. Mensah, G. Lopez, M. Schmela, R. Rossi, W. Hemetsberger and A. Jäger-Waldau, *Prog. Photovoltaics*, 2023, **31**, 1369.
5 P. K. Nayak, S. Mahesh, H. J. Snaith and D. Cahen, *Nat. Rev. Mater.*, 2019, **4**, 269.
6 C. Ballif, F. J. Haug, M. Boccard, P. J. Verlinden and G. Hahn, *Nat. Rev. Mater.*, 2022, **7**, 597.
7 J. Liu, J. Wang, Y. Liu, K. Xian, K. Zhou, J. Wu, S. Li, W. Zhao, Z. Zhou and L. Ye, *J. Mater. Chem. A*, 2023, **11**, 1013.
8 G. Zhang, F. R. Lin, F. Qi, T. Heumüller, A. Distler, H. J. Egelhaaf, N. Li, P. C. Y. Chow, C. J. Brabec, A. K. Y. Jen and H. L. Yip, *Chem. Rev.*, 2022, **122**(18), 14180.
9 A. Wadsworth, M. Moser, A. Marks, M. S. Little, N. Gasparini, C. J. Brabec, D. Baran and I. McCulloch, *Chem. Soc. Rev.*, 2019, **48**, 1596.
10 J. Zhang, J. Hauch and C. J. Brabec, *Acc. Chem. Res.*, 2024, **57**, 1434.
11 W. Lowrie, R. J. E. Westbrook, J. Guo, H. I. Gonev, J. Marin-Beloqui and T. M. Clarke, *J. Chem. Phys.*, 2023, **158**, 110901.
12 S. Hadke, M. Huang, C. Chen, Y. F. Tay, S. Chen, J. Tang and L. Wong, *Chem. Rev.*, 2022, **122**, 10170.
13 Y. Khan, A. Thielens, S. Muin, J. Ting, C. Baumbauer and A. C. Arias, *Adv. Mater.*, 2020, **32**, 1905279.
14 S. K. Karunakaran, G. M. Arumugam, W. Yang, S. Ge, S. Nawaz Khan, X. Lin and G. Yang, Recent progress in inkjet-printed solar cells, *J. Mater. Chem. A*, 2019, **7**, 13873.
15 A. K. Geim and K. S. Novoselov, *Nat. Mater.*, 2007, **6**, 183.
16 Y. Hancock, *J. Phys. D. Appl. Phys.*, 2011, **44**, 473001.
17 D. Jariwala, A. R. Davoyan, J. Wong and H. A. Atwater, *ACS Photonics*, 2017, **4**, 2962.
18 M. Li, J. S. Chen and M. Cotlet, *ACS Energy Lett.*, 2019, **4**, 2323.
19 Z. Qin, Y. Chen, K. Zhu and Y. Zhao, *ACS Mater. Lett.*, 2021, **3**, 1402.
20 P. Kumar, G. Singh, X. Guan, S. Roy, J. Lee, I. Y. Kim, X. Li, F. Bu, R. Bahadur, S. A. Iyengar, J. Yi, D. Zhao, P. M. Ajayan and A. Vinu, *Adv. Mater.*, 2024, **36**, 2403881.
21 E. H. Hill, *J. Mater. Chem. C*, 2024, 11285.
22 U. K. Aryal, M. Ahmadpour, V. Turkovic, H. G. Rubahn, A. Di Carlo and M. Madsen, *Nano Energy*, 2022, **94**, 106833.
23 G. Kakavelakis, E. Kymakis and K. Petridis, *Adv. Mater. Interfaces*, 2018, **5**, 1800339.
24 H. Shao, N. H. Ladi, H. Pan, X. L. Zhang, Y. Shen and M. Wang, *Sol. RRL*, 2021, **5**, 2000566.
25 S. Dongre S, R. Shwetharani, C. Hunsur Ravikumar, C. Lavanya and R. G. Balakrishna, *Adv. Mater. Interfaces*, 2022, **9**, 2200442.
26 Z. Yin, J. Zhu, Q. He, X. Cao, C. Tan, H. Chen, Q. Yan and H. Zhang, *Adv. Energy Mater.*, 2014, **4**, 1300574.

27 T. H. Chowdhury, A. Islam, A. K. Mahmud Hasan, M. A. M. Terdi, M. Arunakumari, S. Prakash Singh, M. K. Alam, I. M. Bedja, M. Hafidz Ruslan, K. Sopian, N. Amin and M. Akhtaruzzaman, *Chem. Rec.*, 2016, **16**, 614.
28 J. Zhang, J. Fan, B. Cheng, J. Yu and W. Ho, *Sol. RRL*, 2020, **4**, 2000502.
29 D. W. Chang, H. J. Choi, A. Filer and J. B. Baek, *J. Mater. Chem. A*, 2014, **2**, 12136.
30 C. Petridis, G. Kakavelakis and E. Kymakis, *Energy Environ. Sci.*, 2018, **11**, 1030.
31 H. Su, T. Wu, D. Cui, X. Lin, X. Luo, Y. Wang and L. Han, *Small Methods*, 2020, **4**, 2000507.
32 E. T. Mombeshora, E. Muchuweni, R. Garcia-Rodriguez, M. L. Davies, V. O. Nyamori and B. S. Martincigh, *Nanoscale Adv.*, 2022, **4**, 2057.
33 Z. Niazi, A. Hagfeldt and E. K. Goharshadi, *J. Mater. Chem. A*, 2023, **11**, 6659.
34 T. Mahmoudi, Y. Wang and Y. B. Hahn, *Nano Energy*, 2018, **47**, 51.
35 J. Liu, M. Durstock and L. Dai, *Energy Environ. Sci.*, 2014, **7**, 1297.
36 J. Pang, A. Bachmatiuk, Y. Yin, B. Trzebicka, L. Zhao, L. Fu, R. G. Mendes, T. Gemming, Z. Liu and M. H. Rummeli, *Adv. Energy Mater.*, 2018, **8**, 1702093.
37 M. Batmunkh, M. Bat-Erdene and J. G. Shapter, *Adv. Mater.*, 2016, **28**, 8586.
38 Z. Shi, R. Khaledialidusti, M. Malaki and H. Zhang, *Nanomaterials*, 2021, **11**, 3170.
39 I. Ali, M. Faraz Ud Din and Z. G. Gu, *Molecules*, 2022, **27**, 3170.
40 S. Kazim, C. Huang, N. H. Hemasiri, A. Kulkarni, S. Mathur and S. Ahmad, *Adv. Funct. Mater.*, 2024, 2315694.
41 M. A. Saeed, A. Shahzad, K. Rasool, F. Mateen, J. M. Oh and J. W. Shim, *Adv. Sci.*, 2022, **9**, 2104743.
42 S. Kumar Singh, A. Kumar Tiwari and H. K. Paliwal, *FlatChem*, 2023, **39**, 100493.
43 S. Aftab, A. Abbas, M. Z. Iqbal, S. Hussain, F. Kabir, H. H. Hegazy, F. Xu, J. H. Kim and B. S. Goud, *Mater. Today Energy*, 2023, **36**, 101366.
44 F. Bonaccorso, Z. Sun, T. Hasan and A. C. Ferrari, *Nat. Photonics*, 2010, **4**, 611.
45 S. Qamar, K. Fatima, N. Ullah, Z. Akhter, A. Waseem and M. Sultan, *Nanoscale*, 2022, **14**, 13018.
46 S. Aftab, M. Z. Iqbal, S. Hussain, F. Kabir, S. Kumar, H. H. Hegazy and B. Sravanthi Goud, *J. Mater. Chem. C*, 2023, **11**, 13189.
47 S. Marimuthu, A. Prabhakaran Shyma, S. Sathyanarayanan, T. Gopal, J. T. James, S. P. Nagalingam, B. Gunaseelan, S. Babu, R. Sellappan and A. N. Grace, *Nanoscale*, 2024, **16**, 10108.
48 D. Lembke, S. Bertolazzi and A. Kis, *Acc. Chem. Res.*, 2015, **48**, 100.
49 A. D. Al-Ghiffari, N. A. Ludin, M. L. Davies, R. M. Yunus and M. S. Suait, *Mater. Today Commun.*, 2022, **32**, 104078.
50 D. Mouloua, A. Kotbi, G. Deokar, K. Kaja, M. El Marssi, M. A. El Khakani and M. Jouiad, *Materials*, 2021, **14**, 3283.
51 E. Singh, K. S. Kim, G. Y. Yeom and H. S. Nalwa, *ACS Appl. Mater. Interfaces*, 2017, **9**, 3223–3245.
52 Y. P. Venkata Subbaiah, K. J. Saji and A. Tiwari, *Adv. Funct. Mater.*, 2016, **26**, 2046.
53 Z. Zhou, J. Lv, C. Tan, L. Yang and Z. Wang, *Adv. Funct. Mater.*, 2024, **34**, 2316175.
54 E. Muchuweni, E. T. Mombeshora, B. S. Martincigh and V. O. Nyamori, *Sol. Energy*, 2022, **239**, 74.
55 Y. Wang, L. Liu, T. Ma, Y. Zhang and H. Huang, *Adv. Funct. Mater.*, 2021, **31**, 2102540.
56 A. G. Ricciardulli and P. W. M. Blom, *Adv. Mater. Technol.*, 2020, **5**, 1900972.
57 Y. Zhao, L. Yu and M. Sun, *Sol. Energy*, 2021, **218**, 621–638.
58 Z. Zhou, J. Lv, C. Tan, L. Yang and Z. Wang, *Adv. Funct. Mater.*, 2024, **34**, 2316175.
59 G. Kakavelakis, E. Kymakis and K. Petridis, *Adv. Mater. Interfaces*, 2018, **5**, 1800339.
60 A. S. R. Bati, M. Batmunkh and J. G. Shapter, *Adv. Energy Mater.*, 2020, **10**, 1902253.
61 S. Suragtkhuu, S. Sunderiya, P. Myagmarsereejid, S. Purevdorj, A. S. R. Bati, B. Bold, Y. L. Zhong, S. Davaasambuu and M. Batmunkh, *Adv. Energy Mater.*, 2023, **13**, 2204074.
62 S. Das, D. Pandey, J. Thomas and T. Roy, *Adv. Mater.*, 2019, **31**, 1802722.
63 S. Bellani, A. Bartolotta, A. Agresti, G. Calogero, G. Grancini, A. Di Carlo, E. Kymakis and F. Bonaccorso, *Chem. Soc. Rev.*, 2021, **50**, 11870–11965.
64 D. K. Sang, H. Wang, Z. Guo, N. Xie and H. Zhang, *Adv. Funct. Mater.*, 2019, **29**, 1903419.
65 S. Cao, J. Low, J. Yu and M. Jaroniec, *Adv. Mater.*, 2015, **27**, 2150.
66 T. S. Miller, A. Belen Jorge, T. M. Suter, A. Sella, F. Cora and P. F. McMillan, *Phys. Chem. Chem. Phys.*, 2017, **19**, 15613.
67 H. Li, J. Wu, Z. Yin and H. Zhang, *Acc. Chem. Res.*, 2014, **47**, 1067.
68 W. Zhang, Q. Wang, Y. Chen, Z. Wang and A. T. S. Wee, *2D Mater.*, 2016, **3**, 022001.
69 X. Huang, Z. Zeng and H. Zhang, *Chem. Soc. Rev.*, 2013, **42**, 1934.
70 X. Wang, J. Song and J. Qu, *Angew. Chem., Int. Ed.*, 2019, **58**, 1574.
71 J. A. Carrasco, P. Congost-Escoin, M. Assebban and G. Abellán, *Chem. Soc. Rev.*, 2023, **52**, 1288.
72 C. Wang, S. Guan, H. Zhang, R. Shen, H. Yuan and B. Li, *APL Mater.*, 2023, **11**, 050902.
73 T. Zhong, L. Zeng, Z. Li, L. Sun, Z. Qiao, Y. Qu, G. Liu and L. Li, *Appl. Sci.*, 2023, **13**, 35.
74 M. Akhtar, G. Anderson, R. Zhao, A. Alruqi, J. E. Mroczkowska, G. Sumanasekera and J. B. Jasinski, *npj 2D Mater. Appl.*, 2017, **1**, 5.
75 L. Jiang, D. Zhou, J. Yang, S. Zhou, H. Wang, X. Yuan, J. Liang, X. Li, Y. Chen and H. Li, *J. Mater. Chem. A*, 2022, **10**, 13651.
76 S. Eigler and A. Hirsch, *Angew. Chem., Int. Ed.*, 2014, **53**, 7720.
77 Y. Gao, C. Lin, K. Zhang, W. Zhou, S. Guo, W. Liu, L. Jiang, S. Zhang and H. Zeng, *Adv. Funct. Mater.*, 2021, **31**, 2102766.
78 J. Nicasio-Collazo, J. L. Maldonado, J. Salinas-Cruz, D. Barreiro-Argüelles, I. Caballero-Quintana, C. Vázquez-Espinosa and D. Romero-Borja, *Opt. Mater.*, 2019, **98**, 109434.
79 L. Yang, C. Dall'Agnese, Y. Dall'Agnese, G. Chen, Y. Gao, Y. Sanehira, A. K. Jena, X. F. Wang, Y. Gogotsi and T. Miyasaka, *Adv. Funct. Mater.*, 2019, **29**, 1905694.
80 A. Agresti, S. Pescetelli, L. Cinà, D. Konios, G. Kakavelakis, E. Kymakis and A. Di Carlo, *Adv. Funct. Mater.*, 2016, **26**, 2686.
81 M. Batmunkh, K. Vimalanathan, C. Wu, A. S. R. Bati, L. P. Yu, S. A. Tawfik, M. J. Ford, T. J. Macdonald, C. L. Raston, S. Priya, C. T. Gibson and J. G. Shapter, *Small Methods*, 2019, **3**, 1800521.
82 P. You, G. Tang, J. Cao, D. Shen, T. W. Ng, Z. Hawash, N. Wang, C. K. Liu, W. Lu, Q. Tai, Y. Qi, C. S. Lee and F. Yan, *Light Sci. Appl.*, 2021, **10**, 23.
83 C. Huang, S. Shi and H. Yu, *ACS Energy Lett.*, 2021, **6**, 3464.
84 U. K. Aryal, H. Pazniak, T. Kumari, M. Weber, F. O. L. Johansson, N. Vannucchi, N. Witkowski, V. Turkovic, A. Di Carlo and M. Madsen, *ACS Appl. Energy Mater.*, 2023, **6**, 4549.
85 Y. Wang, P. Xiang, A. Ren, H. Lai, Z. Zhang, Z. Xuan, Z. Wan, J. Zhang, X. Hao, L. Wu, M. Sugiyama, U. Schwingenschlögl, C. Liu, Z. Tang, J. Wu, Z. Wang and D. Zhao, *ACS Appl. Mater. Interfaces*, 2020, **12**, 53973.
86 P. Myagmarsereejid, S. Suragtkhuu, Q. T. Trinh, T. Gould, N. Nguyen, M. Bat-Erdene, E. Campbell, M. T. Hoang, W. H. Chiu, Q. Li, H. Wang, Y. L. Zhong and M. Batmunkh, *npj 2D Mater. Appl.*, 2024, **8**, 38.
87 T. Chen, G. Tong, E. Xu, H. Li, P. Li, Z. Zhu, J. Tang, Y. Qi and Y. Jiang, *J. Mater. Chem. A*, 2019, **7**, 20597.
88 C. Huang, J. Tian, S. Yang, Y. Zhao and H. Yu, *Nano Energy*, 2023, **115**, 108691.
89 X. Zheng, H. Zhang, Q. Yang, C. Xiong, W. Li, Y. Yan, R. S. Gurney and T. Wang, *Carbon*, 2019, **142**, 156.
90 Q. D. Yang, J. Li, Y. Cheng, H. W. Li, Z. Guan, B. Yu and S. W. Tsang, *J. Mater. Chem. A*, 2017, **5**, 9852.
91 L. Chen, D. Du, K. Sun, J. Hou and J. Ouyang, *ACS Appl. Mater. Interfaces*, 2014, **6**, 22334.
92 F. Zhang, J. He, Y. Xiang, K. Zheng, B. Xue, S. Ye, X. Peng, Y. Hao, J. Lian, P. Zeng, J. Qu and J. Song, *Adv. Mater.*, 2018, **30**, 1803244.
93 A. Saboor, O. Stroyuk, O. Raievska, C. Liu, J. Hauch and C. J. Brabec, *Adv. Funct. Mater.*, 2024, 2400453.
94 J. Liu, Y. Xue and L. Dai, *J. Phys. Chem. Lett.*, 2012, **3**, 1928.
95 Y. Park, K. Soon Choi and S. Young Kim, *Phys. Status Solidi A*, 2012, **209**, 1363.
96 Y. Lin, B. Adilbekova, Y. Firdaus, E. Yengel, H. Faber, M. Sajjad, X. Zheng, E. Yarali, A. Seitkhan, O. M. Bakr, A. El-Labban, U. Schwingenschlögl, V. Tung, I. McCulloch, F. Laquai and T. D. Anthopoulos, *Adv. Mater.*, 2019, **31**, 1902965.
97 R. Xue, X. Zhou, S. Peng, P. Xu, S. Wang, C. Xu, W. Zeng, Y. Xiong and D. Liang, *ACS Sustainable Chem. Eng.*, 2020, **8**, 10714.

98 J. Yoon, H. Sung, G. Lee, W. Cho, N. Ahn, H. S. Jung and M. Choi, *Energy Environ. Sci.*, 2017, **10**, 337.
99 C. Li, Q. Cao, F. Wang, Y. Xiao, Y. Li, J. J. Delaunay and H. Zhu, *Chem. Soc. Rev.*, 2018, **47**, 4981.
100 S. Pei and H. M. Cheng, *Carbon*, 2012, **50**, 3210.
101 D. R. Dreyer, S. Park, C. W. Bielawski and R. S. Ruoff, *Chem. Soc. Rev.*, 2010, **39**, 228.
102 P. Ares, J. J. Palacios, G. Abellán, J. Gómez-Herrero and F. Zamora, *Adv. Mater.*, 2018, **30**, 1703771.
103 L. Ding, P. Shao, Y. Yin and F. Ding, *Adv. Funct. Mater.*, 2024, 2316612.
104 W. Zhang, X. Zhang, L. K. Ono, Y. Qi and H. Oughaddou, *Small*, 2024, **20**, 2303115.
105 L. Ding, P. Shao, Y. Yin and F. Ding, *Adv. Funct. Mater.*, 2024, 2316612.
106 Y. Zhao, L. Yu and M. Sun, *Sol. Energy*, 2021, **218**, 621.
107 Y. Wang, K. Chen, H. Hao, G. Yu, B. Zeng, H. Wang, F. Zhang, L. Wu, J. Li, S. Xiao, J. He, Y. Zhang and H. Zhang, *Nanoscale*, 2019, **11**, 2637.
108 W. Zhen and C. Xue, *Sol. RRL*, 2021, **5**, 2000440.
109 Y. Pang, J. Li, K. Lv, D. Tang and Q. Li, *New J. Chem.*, 2024, **48**, 12477.
110 M. Jiang, D. Wang, Y.-H. Kim, C. Duan, D. Talapin and C. Zhou, *Angew. Chem., Int. Ed.*, 2024, **136**, e202409480.
111 S. Kumar, *Small*, 2024, **20**, 2308225.
112 Y. Wei, P. Zhang, R. A. Soomro, Q. Zhu and B. Xu, *Adv. Mater.*, 2021, **33**, 2103148.
113 Y. L. Huang, Y. Chen, W. Zhang, S. Y. Quek, C. H. Chen, L. J. Li, W. T. Hsu, W. H. Chang, Y. J. Zheng, W. Chen and A. T. S. Wee, *Nat. Commun.*, 2015, **6**, 6298.
114 S. Roy and P. Bermel, *Sol. Energy Mater. Sol. Cells*, 2018, **174**, 370.
115 M. Velický, M. A. Bissett, C. R. Woods, P. S. Toth, T. Georgiou, I. A. Kinloch, K. S. Novoselov and R. A. W. Dryfe, *Nano Lett.*, 2016, **16**, 2023.
116 M. Bernardi, M. Palummo and J. C. Grossman, *Nano Lett.*, 2013, **13**, 3664.
117 X. He, Y. Iwamoto, T. Kaneko and T. Kato, *Sci. Rep.*, 2022, **12**, 11315.
118 Z. Wang, R. Zhang, M. Zhao, Z. Wang, B. Wei, X. Zhang, S. Feng, H. Cao, P. Liu, Y. Hao, H. Wang, B. Xu, S. J. Pennycook and J. Guo, *J. Mater. Chem. A*, 2018, **6**, 23773.
119 S. Y. Kim, S. J. Cho, S. E. Byeon, X. He and H. J. Yoon, *Adv. Energy Mater.*, 2020, **10**, 2002606.
120 K. Li, C. Zhang, M. Zhao, J. Ren, S. Li and Y. Hao, *ACS Appl. Mater. Interfaces*, 2024, **16**, 655.
121 Y. Zhao, X. Zhang, X. Han, C. Hou, H. Wang, J. Qi, Y. Li and Q. Zhang, *Chem. Eng. J.*, 2021, **417**, 127912.
122 M. F. U. Din, S. Sousani, M. Kotlar, S. Ullah, M. Gregor, T. Scepka, Y. Soyka, A. Stepura, A. Shaji, F. Igbari, K. Vegso, V. Nadazdy, P. Siffalovic, M. Jergel, M. Omastova and E. Majkova, *Mater. Today Commun.*, 2023, **36**, 106700.
123 R. Zhang, Z. Huang, W. Chen, B. Lyu, H. Zhang, X. He, X. Hu, Y. Song and W. C. H. Choy, *Adv. Funct. Mater.*, 2023, **33**, 2210063.
124 L. Yang, Z. Liu, T. Zheng, P. Li, J. Ma, X. Zhang, X. F. Wang and Y. Liu, *J. Mater. Chem. A*, 2024, **12**, 21268.
125 L. Kong, X. Cao, K. Liang, R. Wang, J. Liu, W. Shi and C. Lu, *J. Phys. Chem. C*, 2023, **127**, 13493.
126 W. Cao, J. Zhang, K. Lin, L. Qiu, J. Li, Y. Dong, J. Wang, D. Xia, R. Fan and Y. Yang, *Sol. RRL*, 2021, **5**, 2100058.
127 P. Guo, C. Liu, X. Li, Z. Chen, H. Zhu, L. Zhu, X. Zhang, W. Zhao, N. Jia, Q. Ye, X. Xu, R. Chen, Z. Liu, X. Fan, C. Zhi and H. Wang, *Adv. Energy Mater.*, 2022, **12**, 2202395.
128 Y. Wang, J. Li, X. Yao, C. Xie, Q. Chen, W. Liu, Z. Gao, Y. Fu, Q. Liu, D. He and Y. Li, *ACS Appl. Mater. Interfaces*, 2022, **14**, 40930.
129 W. W. Liu, Y. C. Liu, C. Y. Cui, S. T. Niu, W. J. Niu, M. C. Liu, M. J. Liu, B. Gu, L. Y. Zhang, K. Zhao, F. Ran and Y. L. Chueh, *Mater. Today Energy*, 2021, **21**, 100782.
130 D. W. Kim, J. Choi, J. Byun, J. T. Kim, G. S. Lee, J. G. Kim, D. Kim, P. Boonmongkolras, P. F. McMillan, H. M. Lee, A. J. Clancy, B. Shin and S. O. Kim, *ACS Appl. Mater. Interfaces*, 2021, **13**, 61215.
131 J. Bauer, L. S. Quintanar, K. Wang, A. A. Puretzky, K. Xiao, D. B. Geohegan and A. Boulesbaa, *J. Phys. Chem. C*, 2018, **122**, 28910.
132 A. Agresti, A. Pazniak, S. Pescetelli, A. Di Vito, D. Rossi, A. Pecchia, M. Auf der Maur, A. Liedl, R. Larciprete, D. V. Kuznetsov, D. Saranin and A. Di Carlo, *Nat. Mater.*, 2019, **18**, 1228.
133 M. Ashraf, N. H. Hemasiri, S. Kazim, N. Ullah, M. Khan, S. Adewale Ganiyu, K. R. Alhooshani, M. N. Tahir and S. Ahmad, *Sustain. Energy Fuels*, 2022, **7**, 763.
134 F. Biccari, F. Gabelloni, E. Burzi, M. Gurioli, S. Pescetelli, A. Agresti, A. E. Del Rio Castillo, A. Ansaldo, E. Kymakis, F. Bonaccorso, A. Di Carlo and A. Vinattieri, *Adv. Energy Mater.*, 2017, **7**, 1701349.
135 Z. Li, P. Wang, C. Ma, F. Igbari, Y. Kang, K. L. Wang, W. Song, C. Dong, Y. Li, J. Yao, D. Meng, Z. K. Wang and Y. Yang, *J. Am. Chem. Soc.*, 2021, **143**, 2593.
136 J. H. Heo, F. Zhang, J. K. Park, H. Joon Lee, D. S. Lee, S. J. Heo, J. M. Luther, J. J. Berry, K. Zhu and S. H. Im, *Joule*, 2022, **6**, 1672.
137 T. Liu, Y. Liu, M. Chen, X. Guo, S. Tang, R. Zhang, Z. Xie, J. Wang, A. Gu, S. Lin and N. Wang, *Adv. Funct. Mater.*, 2022, **32**, 2106779.
138 S. S. Li, K. H. Tu, C. C. Lin, C. W. Chen and M. Chhowalla, *ACS Nano*, 2010, **4**, 3169.
139 X. Liu, H. Kim and L. J. Guo, *Org. Electron.*, 2013, **14**, 591.
140 W. Lan, J. Gu, S. Wu, Y. Peng, M. Zhao, Y. Liao, T. Xu, B. Wei, L. Ding and F. Zhu, *EcoMat*, 2021, **3**, e12134.
141 Z. Xia, Y. Sun, Y. Jiang, L. Chen, C. Zhao, C. Dai, Z. Wei, G. Zhang, Y. Yu, H. Wang, Z. Z. Zhang, J. Xie, S. Zhou, Q. Zhang, X. Li, J. Shuai, C. Yang and S. Liu, *J. Phys. Chem. Lett.*, 2023, **14**, 6532.
142 N. H. Hemasiri, M. Ashraf, S. Kazim, R. Graf, R. Berger, N. Ullah, M. N. Tahir and S. Ahmad, *Nano Energy*, 2023, **109**, 108326.
143 M. A. Saeed, Z. Khalid, M. J. Lee, H. Ahn, J. M. Oh and J. W. Shim, *Chem. Eng. J.*, 2024, **495**, 153404.
144 B. Deng, H. Lian, B. Xue, R. Song, S. Chen, Z. Wang, T. Xu, H. Dong and S. Wang, *Small*, 2023, **19**, 2207505.
145 S. Kohnehpoushi, P. Nazari, B. A. Nejand and M. Eskandari, *Nanotechnology*, 2018, **29**, 2050201.
146 B. Adilbekova, Y. Lin, E. Yengel, H. Faber, G. Harrison, Y. Firdaus, A. El-Labban, D. H. Anjum, V. Tung and T. D. Anthopoulos, *J. Mater. Chem. C*, 2020, **8**, 5259.
147 W. Lan, X. Gao, Y. Liu, J. Gu, M. Zhao, B. Wei and F. Zhu, *Org. Electron.*, 2021, **93**, 106163.
148 Y. Xu, H. Zhang, Y. Jing, X. Wang, J. Gan, Z. Yan, X. Liu, J. Wu and Z. Lan, *Appl. Surf. Sci.*, 2023, **619**, 156674.
149 Y. Qi, M. A. Sadi, D. Hu, M. Zheng, Z. Wu, Y. Jiang and Y. P. Chen, *Adv. Mater.*, 2023, **35**, 2205714.
150 Q. Ma, G. Ren, K. Xu and J. Z. Ou, *Adv. Opt. Mater.*, 2021, **9**, 2001313.
151 Y. Cai, G. Zhang and Y. W. Zhang, *Sci. Rep.*, 2014, **4**, 6677.
152 J. Kern, A. Trügler, I. Niehues, J. Ewering, R. Schmidt, R. Schneider, S. Najmaei, A. George, J. Zhang, J. Lou, U. Hohenester, S. Michaelis De Vasconcellos and R. Bratschitsch, *ACS Photonics*, 2015, **2**, 1260.
153 J. Cui, S. Liang and J. Zhang, *Phys. Chem. Chem. Phys.*, 2016, **18**, 25388.
154 D. ÇakIr, H. Sahin and F. M. Peeters, *Phys. Rev. B: Condens. Matter Mater. Phys.*, 2014, **90**, 205421.
155 A. R. Khan, T. Lu, W. Ma, Y. Lu and Y. Liu, *Adv. Electron. Mater.*, 2020, **6**, 1901381.
156 J. O. Island, A. Kuc, E. H. Diependaal, R. Bratschitsch, H. S. J. Van Der Zant, T. Heine and A. Castellanos-Gomez, *Nanoscale*, 2016, **8**, 2589.
157 L. Sygellou, G. Paterakis, C. Galiotis and D. Tasis, *J. Phys. Chem. C*, 2016, **120**, 281.
158 O. L. Stroyuk, N. S. Andryushina, S. Y. Kuchmiy and V. D. Pokhodenko, *Theor. Exp. Chem.*, 2015, **51**, 1.
159 J. K. Chang, W. H. Lin, J. I. Taur, T. H. Chen, G. K. Liao, T. W. Pi, M. H. Chen and C. I. Wu, *ACS Appl. Mater. Interfaces*, 2015, **7**, 17155.
160 A. E. Mansour, M. M. Said, S. Dey, H. Hu, S. Zhang, R. Munir, Y. Zhang, K. Moudgil, S. Barlow, S. R. Marder and A. Amassian, *Adv. Funct. Mater.*, 2017, **27**, 1602004.
161 S. Ji, B. K. Min, S. K. Kim, S. Myung, M. Kang, H. S. Shin, W. Song, J. Heo, J. Lim, K. S. An, I. Y. Lee and S. S. Lee, *Appl. Surf. Sci.*, 2017, **419**, 252.
162 E. Stratakis, K. Savva, D. Konios, C. Petridis and E. Kymakis, *Nanoscale*, 2014, **6**, 6925.
163 D. Konios, G. Kakavelakis, C. Petridis, K. Savva, E. Stratakis and E. Kymakis, *J. Mater. Chem. A*, 2016, **4**, 1612.
164 C. Y. Lee, Q. Van Le, C. Kim and S. Y. Kim, *Phys. Chem. Chem. Phys.*, 2015, **17**, 9369.
165 T. Liu, D. Kim, H. Han, A. R. Bin Mohd Yusoff and J. Jang, *Nanoscale*, 2015, **7**, 10708.

166 G. Kakavelakis, D. Konios, E. Stratakis and E. Kymakis, *Chem. Mater.*, 2014, **26**, 5988.
167 J. Liu, Y. Xue, Y. Gao, D. Yu, M. Durstock and L. Dai, *Adv. Mater.*, 2012, **24**, 2228.
168 S. Pareek, S. Waheed and S. Karak, *ACS Appl. Energy Mater.*, 2023, **6**, 554.
169 Z. Yu, W. Feng, W. Lu, B. Li, H. Yao, K. Zeng and J. Ouyang, *J. Mater. Chem. A*, 2019, **7**, 11160.
170 C. Hou, C. Huang, H. Yu and S. Shi, *Small*, 2022, **18**, 2201046.
171 J. K. El-Demellawi, A. E. Mansour, A. M. El-Zohry, M. N. Hedhili, J. Yin, A. H. M. Emwas, P. Maity, X. Xu, O. M. Bakr, O. F. Mohammed and H. N. Alshareef, *ACS Mater. Lett.*, 2022, **4**, 2480.
172 J. Vida, P. Gemeiner, M. Pavličková, M. Mazalová, P. Souček, D. Plašienka and T. Homola, *Nanoscale*, 2023, **15**, 1289.
173 L. Yang, D. Kan, C. Dall'Agnese, Y. Dall'Agnese, B. Wang, A. K. Jena, Y. Wei, G. Chen, X. F. Wang, Y. Gogotsi and T. Miyasaka, *J. Mater. Chem. A*, 2021, **9**, 5016.
174 H. Jing, H. Yeo, B. Lyu, J. Ryou, S. Choi, J. H. Park, B. H. Lee, Y. H. Kim and S. Lee, *ACS Nano*, 2021, **15**, 1388.
175 T. Schultz, N. C. Frey, K. Hantanasirisakul, S. Park, S. J. May, V. B. Shenoy, Y. Gogotsi and N. Koch, *Chem. Mater.*, 2019, **31**, 6590.
176 S. Hu, F. Li, Z. Fan, F. Wang, Y. Zhao and Z. Lv, *Dalton Trans.*, 2014, **44**, 1084.
177 J. Hong, X. Xia, Y. Wang and R. Xu, *J. Mater. Chem.*, 2012, **22**, 15006.
178 D. Liu, C. Li, C. Zhao, Q. Zhao, T. Niu, L. Pan, P. Xu, F. Zhang, W. Wu and T. Ni, *Chem. Eng. J.*, 2022, **438**, 135623.
179 X. Wang, J. Meng, X. Zhang, Y. Liu, M. Ren, Y. Yang and Y. Guo, *Adv. Funct. Mater.*, 2021, **31**, 2010763.
180 S. Y. Lee, U. J. Kim, J. Chung, H. Nam, H. Y. Jeong, G. H. Han, H. Kim, H. M. Oh, H. Lee, H. Kim, Y. G. Roh, J. Kim, S. W. Hwang, Y. Park and Y. H. Lee, *ACS Nano*, 2016, **10**, 6100.
181 M. Y. Tsai, S. Zhang, P. M. Campbell, R. R. Dasari, X. Ba, A. Tarasov, S. Graham, S. Barlow, S. R. Marder and E. M. Vogel, *Chem. Mater.*, 2017, **29**, 7296.
182 A. Tarasov, S. Zhang, M. Y. Tsai, P. M. Campbell, S. Graham, S. Barlow, S. R. Marder and E. M. Vogel, *Adv. Mater.*, 2015, **27**, 1175.
183 S. Zhang, H. M. Hill, K. Moudgil, C. A. Richter, A. R. Hight Walker, S. Barlow, S. R. Marder, C. A. Hacker and S. J. Pookpanratana, *Adv. Mater.*, 2018, **30**, 1802991.
184 J. R. Brent, N. Savjani and P. O'Brien, *Prog. Mater. Sci.*, 2017, **89**, 411.
185 Y. Sozen, J. J. Riquelme, Y. Xie, C. Munuera and A. Castellanos-Gomez, *Small Methods*, 2023, **7**, 2300326.
186 L. Niu, J. N. Coleman, H. Zhang, H. Shin, M. Chhowalla and Z. Zheng, *Small*, 2016, **12**, 272.
187 L. Maggini and R. R. Ferreira, *J. Mater. Chem. C*, 2021, **9**, 15721.
188 Y. Hernandez, V. Nicolosi, M. Lotya, F. M. Blighe, Z. Sun, S. De, I. T. McGovern, B. Holland, M. Byrne, Y. K. Gun'ko, J. J. Boland, P. Niraj, G. Duesberg, S. Krishnamurthy, R. Goodhue, J. Hutchison, V. Scardaci, A. C. Ferrari and J. N. Coleman, *Nat. Nanotechnol.*, 2008, **3**, 563.
189 A. B. Bourlinos, V. Georgakilas, R. Zboril, T. A. Sterioti and A. K. Stubos, *Small*, 2009, **5**, 1841.
190 A. Elbourne, B. McLean, K. Voïtchovsky, G. G. Warr and R. Atkin, *J. Phys. Chem. Lett.*, 2016, **7**, 3118.
191 M. Matsumoto, Y. Saito, C. Park, T. Fukushima and T. Aida, *Nat. Chem.*, 2015, **7**, 730.
192 N. Behabtu, J. R. Lomeda, M. J. Green, A. L. Higginbotham, A. Sinitskii, D. V. Kosynkin, D. Tsentalovich, A. N. G. Parra-Vasquez, J. Schmidt, E. Kesselman, Y. Cohen, Y. Talmon, J. M. Tour and M. Pasquali, *Nat. Nanotechnol.*, 2010, **5**, 406.
193 Z. Li, R. J. Young, C. Backes, W. Zhao, X. Zhang, A. A. Zhukov, E. Tillotson, A. P. Conlan, F. Ding, S. J. Haigh, K. S. Novoselov and J. N. Coleman, *ACS Nano*, 2020, **14**, 10976.
194 Y. V. Panasiuk, A. E. Raevskaya, O. L. Stroyuk, P. M. Lytvyn and S. Y. Kuchmiy, *RSC Adv.*, 2015, **5**, 46843.
195 O. Stroyuk, O. Raievska and D. R. T. Zahn, *Phys. Chem. Chem. Phys.*, 2021, **23**, 20745.
196 M. Shekhirev, J. Busa, C. E. Shuck, A. Torres, S. Bagheri, A. Sinitskii and Y. Gogotsi, *ACS Nano*, 2022, **16**, 13695.
197 J. Kim, G. Yoon, J. Kim, H. Yoon, J. Baek, J. H. Lee, K. Kang and S. Jeon, *Carbon*, 2018, **139**, 309.
198 I. Jeon, B. Yoon, M. He and T. M. Swager, *Adv. Mater.*, 2018, **30**, 1704538.
199 A. E. Del Rio Castillo, V. Pellegrini, A. Ansaldo, F. Ricciardella, H. Sun, L. Marasco, J. Buha, Z. Dang, L. Gagliani, E. Lago, N. Curreli, S. Gentiluomo, F. Palazon, M. Prato, R. Oropesa-Nuñez, P. S. Toth, E. Mantero, M. Crugliano, A. Gamucci, A. Tomadin, M. Polini and F. Bonaccorso, *Mater. Horiz.*, 2018, **5**, 890.
200 N. S. Andryushina, O. L. Stroyuk, I. B. Yanchuk and A. V. Yefanov, *Colloids Polym. Sci.*, 2014, **292**, 539.
201 G. Li, L. Li, H. Yuan, H. Wang, H. Zeng and J. Shi, *J. Colloid Interface Sci.*, 2017, **495**, 19.
202 X. She, H. Xu, Y. Xu, J. Yan, J. Xia, L. Xu, Y. Song, Y. Jiang, Q. Zhang and H. Li, *J. Mater. Chem. A*, 2014, **2**, 2563.
203 Y. Wang, P. Du, H. Pan, L. Fu, Y. Zhang, J. Chen, Y. Du, N. Tang and G. Liu, *Adv. Mater.*, 2019, **31**, 1807540.
204 N. Lu, C. Wang, B. Sun, Z. Gao and Y. Su, *Sep. Purif. Technol.*, 2017, **186**, 226.
205 H. Wang, Y. Su, H. Zhao, H. Yu, S. Chen, Y. Zhang and X. Quan, *Environ. Sci. Technol.*, 2014, **48**, 11984.
206 H. Zhao, H. Yu, X. Quan, S. Chen, H. Zhao and H. Wang, *RSC Adv.*, 2014, **4**, 624.
207 O. Stroyuk, O. Raievska, C. B. Brabec, V. Dzhagan, Y. Havrylyuk and D. R. T. Zahn, *Nanoscale*, 2022, **14**, 12347.
208 O. Stroyuk, O. Raievska, D. R. T. Zahn and C. J. Brabec, *Chem. Rec.*, 2024, **24**, e202300241.
209 S. K. Lee, D. Chu, D. Y. Song, S. W. Pak and E. K. Kim, *Nanotechnology*, 2017, **28**, 195703.
210 Y. Li, Y. Lu, P. Adelhelm, M. M. Titirici and Y. S. Hu, *Chem. Soc. Rev.*, 2019, **48**, 4655.
211 M. Li, W. Ni, B. Kan, X. Wan, L. Zhang, Q. Zhang, G. Long, Y. Zuo and Y. Chen, *Phys. Chem. Chem. Phys.*, 2013, **15**, 18973.
212 H. S. S. Ramakrishna Matte, A. Gomathi, A. K. Manna, D. J. Late, R. Datta, S. K. Pati and C. N. R. Rao, *Angew. Chem., Int. Ed.*, 2010, **49**, 4059.
213 N. H. Kwon, S. J. Shin, X. Jin, Y. Jung, G. S. Hwang, H. Kim and S. J. Hwang, *Appl. Catal., B*, 2020, **277**, 119191.
214 Q. Q. Yang, R. T. Liu, C. Huang, Y. F. Huang, L. F. Gao, B. Sun, Z. P. Huang, L. Zhang, C. X. Hu, Z. Q. Zhang, C. L. Sun, Q. Wang, Y. L. Tang and H. L. Zhang, *Nanoscale*, 2018, **10**, 21106.
215 F. Cheng, H. Wang and X. Dong, *Chem. Commun.*, 2015, **51**, 7176.
216 X. Zhang, H. Wang, H. Wang, Q. Zhang, J. Xie, Y. Tian, J. Wang and Y. Xie, *Adv. Mater.*, 2014, **26**, 4438.
217 B. Szczesniak, S. Borysiuk, J. Choma and M. Jaroniec, *Mater. Horiz.*, 2020, **7**, 1457.
218 S. Iravani, A. Zarepour, E. Nazarzadeh Zare, P. Makvandi, A. Khosravi, R. S. Varma and A. Zarrabi, *Mater. Adv.*, 2024, **5**, 8404.
219 F. Zhou, S. Li, L. Ouyang, J. Liu, J. Liu, Z. Huang and M. Zhu, *Chem. Eng. J.*, 2022, **444**, 136593.
220 O. Y. Posudievsky, O. A. Khazieieva, V. V. Cherepanov, V. G. Koshechko and V. D. Pokhodenko, *J. Nanopart. Res.*, 2013, **15**, 2046.
221 O. Y. Posudievsky, O. A. Kozarenko, V. S. Dyadyun, V. G. Koshechko and V. D. Pokhodenko, *Electrocatalysis*, 2019, **10**, 477.
222 O. Y. Posudievsky, O. A. Khazieieva, V. V. Cherepanov, G. I. Dovbeshko, A. G. Shkavro, V. G. Koshechko and V. D. Pokhodenko, *J. Mater. Chem. C*, 2013, **1**, 6411.
223 O. Y. Posudievsky, O. A. Kozarenko, O. A. Khazieieva, V. G. Koshechko and V. D. Pokhodenko, *J. Mater. Chem. C*, 2013, **1**, 6658.
224 O. Y. Posudievsky, O. A. Khazieieva, V. G. Koshechko and V. D. Pokhodenko, *J. Mater. Chem.*, 2012, **22**, 12465.
225 B. Hu, Y. Wu, K. Wang, H. Guo, Z. Lei, Z. Liu and L. Wang, *Small*, 2024, **20**, 2305344.
226 C. Zhang, Y. Luo, J. Tan, Q. Yu, F. Yang, Z. Zhang, L. Yang, H. M. Cheng and B. Liu, *Nat. Commun.*, 2020, **11**, 3724.
227 C. Zhang, J. Tan, Y. Pan, X. Cai, X. Zou, H. M. Cheng and B. Liu, *Nat. Sci. Rev.*, 2020, **7**, 324.
228 A. M. Abdelkader, A. J. Cooper, R. A. W. Dryfe and I. A. Kinloch, *Nanoscale*, 2015, **7**, 6944.
229 F. Liu, C. Wang, X. Sui, M. A. Riaz, M. Xu, L. Wei and Y. Chen, *Carbon Energy*, 2019, **1**, 173.
230 Y. Yang, H. Hou, G. Zou, W. Shi, H. Shuai, J. Li and X. Ji, *Nanoscale*, 2019, **11**, 16.

231 M. J. Molaei, M. Younas and M. Rezakazemi, *Mater. Sci. Eng. B*, 2022, **285**, 115936.
232 H. W. Guo, Z. Hu, Z. B. Liu and J. G. Tian, *Adv. Funct. Mater.*, 2021, **31**, 2007810.
233 Y. Liu, Y. Huang and X. Duan, *Nature*, 2019, **567**, 323.
234 A. K. Geim and I. V. Grigorieva, *Nature*, 2013, **499**, 419.
235 G. H. Jeong, S. P. Sasikala, T. Yun, G. Y. Lee, W. J. Lee and S. O. Kim, *Adv. Mater.*, 2020, **32**, 1907006.
236 Z. Yuan, X. Xiao, J. Li, Z. Zhao, D. Yu and Q. Li, *Adv. Sci.*, 2018, **5**, 1700626.
237 H. Shi, M. Li, S. Fu, C. Neumann, X. Li, W. Niu, Y. Lee, M. Bonn, H. I. Wang, A. Turchanin, A. Shaygan Nia, S. Yang and X. Feng, *Angew. Chem.*, 2023, **135**, e202303929.
238 B. Sa, R. Hu, Z. Zheng, R. Xiong, Y. Zhang, C. Wen, J. Zhou and Z. Sun, *Chem. Mater.*, 2022, **34**, 6687.
239 J. Linghu, T. Yang, Y. Luo, M. Yang, J. Zhou, L. Shen and Y. P. Feng, *ACS Appl. Mater. Interfaces*, 2018, **10**, 32142.
240 Y. Ding, Z. Huang, C. Di, H. Wang, Y. Xin, B. Sun, J. Chen, Y. Xu, D. Wei and G. Fu, *Sol. RRL*, 2023, **7**, 2300250.
241 Y. Ma, P. M. Ajayan, S. Yang and Y. Gong, *Small*, 2018, **14**, 1801606.
242 L. Zhou, D. Yang, W. Yu, J. Zhang and C. Li, *Org. Electron.*, 2015, **23**, 110.
243 M. Q. Yang, Y. J. Xu, W. Lu, K. Zeng, H. Zhu, Q. H. Xu and G. W. Ho, *Nat. Commun.*, 2017, **8**, 14224.
244 H. C. Cheng, G. Wang, D. Li, Q. He, A. Yin, Y. Liu, H. Wu, M. Ding, Y. Huang and X. Duan, *Nano Lett.*, 2016, **16**, 367.
245 L. Shen, J. Zhou, T. Yang, M. Yang and Y. P. Feng, *Acc. Mater. Res.*, 2022, **3**, 572.
246 X. Zhang, A. Chen, L. Chen and Z. Zhou, *Adv. Energy Mater.*, 2022, **12**, 2003841.
247 R. Khaledialidusti, M. Khazaei, S. Khazaei and K. Ohno, *Nanoscale*, 2021, **13**, 7294.
248 X. Jia, Q. Shao, Y. Xu, R. Li, K. Huang, Y. Guo, C. Qu and E. Gao, *npj Comput. Mater.*, 2021, **7**, 211.
249 N. Mounet, M. Gibertini, P. Schwaller, D. Campi, A. Merkys, A. Marrazzo, T. Sohier, I. E. Castelli, A. Cepellotti, G. Pizzi and N. Marzari, *Nat. Nanotechnol.*, 2018, **13**, 246.
250 J. Zhou, L. Shen, M. D. Costa, K. A. Persson, S. P. Ong, P. Huck, Y. Lu, X. Ma, Y. Chen, H. Tang and Y. P. Feng, *Sci. Data*, 2019, **6**, 86.
251 V. Wang, G. Tang, Y. C. Liu, R. T. Wang, H. Mizuseki, Y. Kawazoe, J. Nara and W. T. Geng, *J. Phys. Chem. Lett.*, 2022, **13**, 11581.
252 S. Pakdel, A. Rasmussen, A. Taghizadeh, M. Kruse, T. Olsen and K. S. Thygesen, *Nat. Commun.*, 2024, **15**, 932.
253 Y. Li, L. Su, Y. Lu, Q. Luo, P. Liang, H. Shu and X. Chen, *InfoMat*, 2023, **5**, e12407.
254 X. Liu, P. Gao, W. Hu and J. Yang, *J. Phys. Chem. Lett.*, 2020, **11**, 4070.
255 R. K. Barik and L. M. Woods, *Sci. Data*, 2023, **10**, 232.
256 P. Huang, R. Lukin, M. Faleev, N. Kazeev, A. R. Al-Maeeni, D. V. Andreeva, A. Ustyuzhanin, A. Tormasov, A. H. Castro Neto and K. S. Novoselov, *npj 2D Mater. Appl.*, 2023, **7**, 6.